China Geology 5 (2022) 696−721

China Geology

Journal homepage: http://chinageology.cgs.cn
https://www.sciencedirect.com/journal/china-geology

Geology and mineralization of the Dayin'gezhuang supergiant gold deposit (180 t) in the Jiaodong Peninsula, China: A review

Xiang-dong Liu[a, b, c], Zheng-jiang Ding[a, b,*], Ming-chun Song[d], Ming-ling Zhou[a, b], Shao-hui Xu[a, b], Zhen-liang Yang[a, b], Tian-ci Xie[a, b], Tao Cui[c], Ying-xin Song[e], Xue-kan Gao[f], Rui-xiang Li[a, b], Liang-liang Zhang[a, b], Qi-bin Zhang[a, b], Shan-shan Wang[a, b], Bin Wang[a, b]

[a] *No.6 Geological Team of Shandong Provincial Bureau of Geology and Mineral Resources, Weihai* 264209, *China*
[b] *Ministry of Natural Resources Technology Innovation Center for Deep Gold Resources Exploration and Mining, Weihai* 264209, *China*
[c] *State Key Laboratory of Geological Process and Mineral Resources, China University of Geosciences (Beijing), Beijing* 100083, *China*
[d] *Hebei Key Laboratory of Strategic Critical Mineral Resources, Hebei GEO University, Shijiazhuang* 050031, *China*
[e] *Shandong Institute of Geological Sciences, Jinan* 250013, *China*
[f] *Dayin'gezhuang Gold Company, Zhaojin Mining Co., Ltd., Zhaoyuan* 264000, *China*

ARTICLE INFO

Article history:
Received 30 September 2022
Received in revised form 13 October 2022
Accepted 20 October 2022
Available online 25 October 2022

Keywords:
Stepped metallogenic model
Thermal uplifting-extension mineralization
Geological characteristics
Supergiant gold deposit
Zhaoping metallogenic belt
Jiaodong gold province
Mineral exploration engineering
Dayin'gezhuang
Shandong Province
China

ABSTRACT

The Dayin'gezhuang gold deposit is located in the central part of the Zhaoping Fault metallogenic belt in the Jiaodong gold province—the world's third-largest gold metallogenic area. It is a typical successful case of prospecting at a depth of 500–2000 m in recent years, with cumulative proven gold resources exceeding 180 t. The main orebodies (No. 1 and No. 2 orebody) generally have a pitch direction of NNE and a plunge direction of NEE. As the ore-controlling fault, the Zhaoping Fault is a shovel-shaped stepped fault, with its dip angle presenting stepped high-to-low transitions at the elevation of −2000–0 m. The gold mineralization enrichment area is mainly distributed in the step parts where the fault plane changes from steeply to gently, forming a stepped metallogenic pattern from shallow to deep. It can be concluded from previous studies that the gold mineralization of the Dayin'gezhuang gold deposit occurred at about 120 Ma. The ore-forming fluids were H_2O-CO_2-NaCl-type hydrothermal solutions with a medium-low temperature and medium-low salinity. The H-O isotopic characteristics indicate that the fluids in the early ore-forming stage were possibly magmatic water or mantle water and that meteoric water gradually entered the ore-forming fluids in the late ore-forming stage. The S and Pb isotopes indicate that the ore-forming materials mainly originate from the lower crust and contain a small quantity of mantle-derived components. The comprehensive analysis shows that the Dayin'gezhuang gold deposit was formed by thermal uplifting-extensional tectonism. The strong crust-mantle interactions, large-scale magmatism, and the material exchange arising from the transformation from adakitic granites to arc granites and from the ancient lower crust to the juvenile lower crust during the Early Cretaceous provided abundant fluids and material sources for mineralization. Moreover, the detachment faults formed by the rapid magmatic uplift and the extensional tectonism created favorable temperature and pressure conditions and space for fluid accumulation and gold precipitation and mineralization.

1. Introduction

The Jiaodong gold province, with more than 5000 t of proven gold resources, is the world's third-largest gold metallogenic area, where three kiloton-class gold orefields, i.e., Sanshandao, Jiaojia, and Linglong, have been successively discovered (Deng J et al., 2019; Song MC et al., 2021a, 2022a; Yue XF et al., 2020). The Dayin'gezhuang gold deposit is located in the central part of the Zhaoping Fault metallogenic belt in the Jiaodong gold province. More than 50 t of gold resources were discovered in this deposit in the 1970s. With the implementation of the strategy for deep deposit prospecting and the National Exploration & Development Planning, great progress has been made in the

First author: *E-mail address*: 877369082@qq.com (Xiang-dong Liu).

* Corresponding author: *E-mail address*: ytdzhj@126.com (Zheng-jiang Ding).

Literary editor: Li-qiong Jia
doi:10.31035/cg2022058
2096-5192/© 2022 China Geology Editorial Office.

deep and peripheral prospecting of the Dayin'gezhuang gold deposit since the 21st century. At present, this deposit has cumulative proven gold resources of more than 180 t, making it the largest gold deposit in the central portion of the Zhaoping Fault zone.

A lot of studies have been conducted on the Dayin'gezhuang gold deposit (Li H et al., 1998; Shen K et al., 2000; Li DX et al., 2006; Wang QF et al., 2007; Yang LQ et al., 2009; Deng J et al., 2011; Yang LQ et al., 2014a; Liu Y et al., 2014; Zhang L et al., 2014; Zhang RZ et al., 2016; Zhang BL et al., 2017; Chai P et al., 2019a, 2019b; Mao XC et al., 2019, 2020; Yuan ZZ et al., 2019; Chen J et al., 2020a, 2020b; Deng H et al., 2020; Wei YJ et al., 2020, 2022; Shen YK et al., 2022; Xie TC et al., 2022), achieving many important results on ore-controlling factors, alteration and mineralization characteristics, metallogenic age, ore-forming stages, ore deposit geochemistry, ore-forming fluids, and ore-forming material sources. However, previous studies are mainly based on the exploration results at an elevation of −800–0 m, while lacking systematic analysis of deep metallogenic characteristics and the spatial occurrence patterns of orebodies. In recent years, the authors of this paper have completed gold exploration at an elevation of −2000–0 m in the Dayin'gezhuang gold deposit and systematically revealed the deep characteristics of the deposit. This paper systematically reviewed the main achievements in shallow prospecting in the past and deep prospecting in recent years in the Dayin'gezhuang gold deposit, expatiated the main characteristics of the deposit, analyzed the spatial distribution and deep variations of orebodies, and summarized the previous study results on metallogenic age and ore deposit geochemistry. Based on these, the ore-controlling regularity of faults and the metallogenic age were analyzed, the properties and sources of the ore-forming fluids and the sources of the ore-forming materials were discussed, and the genetic model of the Dayin'gezhuang gold deposit was finally proposed. This paper is significant for deeply understanding the metallogenic regularity and formation mechanisms of Jiaodong gold deposits and for guiding deep prospecting. Moreover, it provides a typical model for deepening research on the mineralization of the Jiaodong gold deposits—Mesozoic gold deposits in the Precambrian metamorphic basement.

2. Regional geology

The Jiaodong gold province, where the Dayin'gezhuang gold deposit is located, experienced multi-phase tectonic superposition. In particular, the strong Yanshanian tectono-magmatic movement caused the Mesozoic metallogenic explosion (Mao JW et al., 1999; Zhai MG et al., 2004). The Jiaodong Peninsula is mainly composed of two tectonic units, i.e., the Jiaobei Terrane in the North China Plate and the Sulu Terrane in the Qinling-Dabie-Sulu Orogen (Fig. 1; Yang LQ et al., 2014b; Deng J et al, 2020a, 2020b; Fan HR et al., 2021). The Jiaobei Terrane, located on the southeastern margin of the North China Plate, consists of the Jiaobei uplift in the north and the Jiaolai Basin in the south. The Sulu Terrane, located on the northeastern margin of the Qinling-Dabie-Sulu Orogen, mainly consists of the Weihai uplift. The Jiaobei uplift is mainly composed of Precambrian

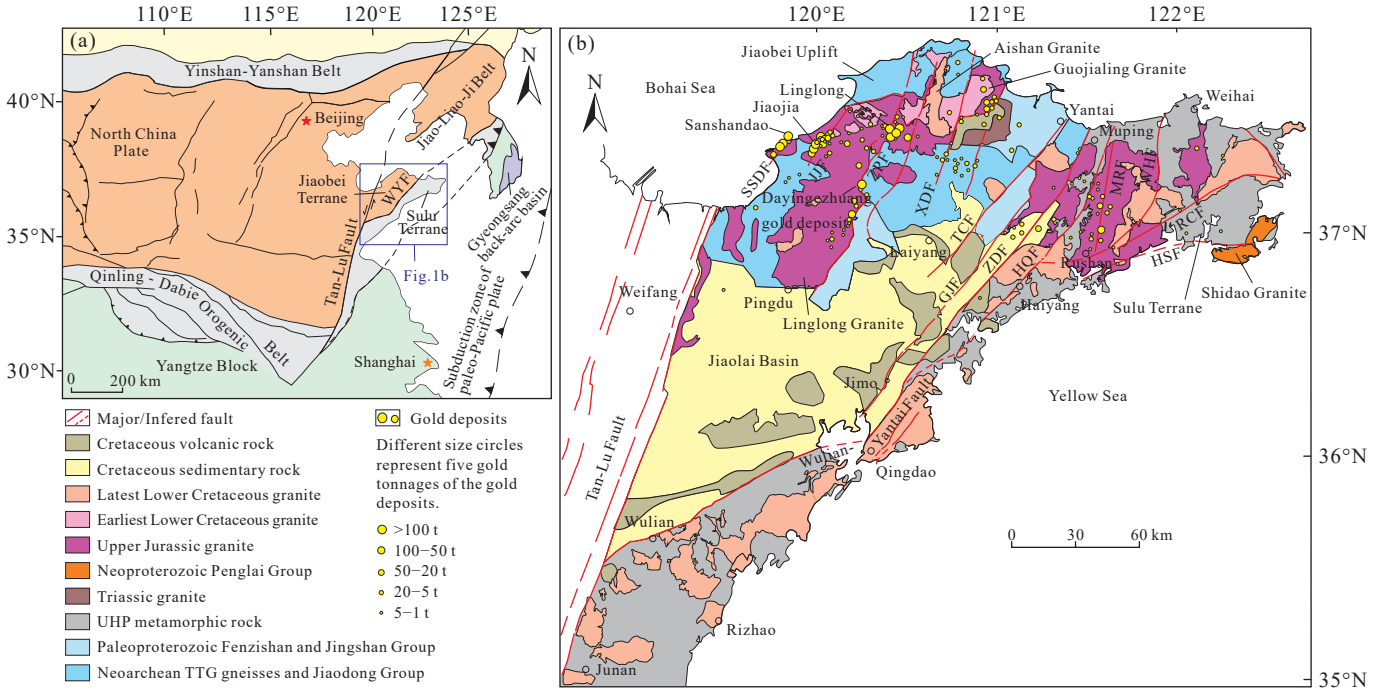

Fig. 1. a–Regional geological sketch map; b–geological map of the Jiaodong gold province showing the distribution of gold deposits in terms of size (modified from Chough SK et al. 2010; Deng J et al. 2020a, 2020b; Song MC et al. 2020a). GJF–Guocheng-Jimo Fault; HQF–Haiyang-Qingdao Fault; HSF–Haiyang-Shidao Fault; JJF–Jiaojia Fault; MRF–Muping-Rushan Fault; RCF–Rongcheng Fault; SSDF–Sanshandao Fault; TCF–Taocun Fault; WHF–Weihai Fault; WYF–Wulian-Yantai Fault; XDF–Xilin-Douya Fault; ZDF–Zhuwu-Dianji Fault; ZPF–Zhaoping Fault.

metamorphic basement rocks and Mesozoic intrusions, with a small amount of Paleogene-Neogene volcanic rocks and clastic sediments and Quaternary loose sediments distributed in the coastal area. The Precambrian metamorphic basement is mainly composed of the amphibolites (metagabbros), biotite leptynites, and plagiogneisses of the Neoarchean Jiaodong Group, the Neoarchean gneisses of tonalite-trondhjemite-granodiorite (TTG) affinity (the TTG gneisses), the marbles, schists, diopsides, and leptynites of the Paleoproterozoic Jingshan and Fenzishan groups, and the metamorphic sedimentary rocks of both the Mesoproterozoic Zhifu Group and the Neoproterozoic Penglai Group. The Jiaolai Basin is a Cretaceous continental basin composed of continental volcanic-sedimentary rocks, including the Early Cretaceous Laiyang and Qingshan groups and the Late Cretaceous–Paleocene Wangshi Group (Li SJ et al., 1998; Li JL et al., 2007; Ren FL et al., 2008). The Weihai uplift, as a part of the Triassic collisional orogenic belt between the North China Plate and the Yangtze Block, is mainly composed of the ultrahigh-pressure metamorphic belts and Mesozoic intrusions. The ultrahigh-pressure metamorphic belt is mainly composed of Neoproterozoic granitic gneisses and a small quantity of Neoarchean-Paleoproterozoic metamorphic supracrustal rocks and is interbedded with eclogites and mafic-ultramafic rock lenses (Ames L et al., 1996; Liu LS et al., 2018). This metamorphic belt underwent eclogite-facies ultrahigh-pressure metamorphism at 240–220 Ma (Wallis et al., 1999). Mesozoic intrusions are widely distributed in the Jiaodong area and can be divided into Upper Triassic granites (Shidao rocks; Chen JF et al., 2003; Gao TS et al., 2004; Guo JH et al., 2005; Chen JZ and Jiang N, 2011), Upper Jurassic granites (Linglong and Wendeng granites; Zhang J et al., 2010; Jiang N et al., 2012; Ma L et al., 2013; Yang LQ et al., 2018), Earliest Lower Cretaceous granodiorites (Guojialing granites; Liu Y et al., 2014; Geng K et al., 2016), and Latest Lower Cretaceous granites (Weideshan and Laoshan granites; Guo JH et al., 2005; Goss SC et al., 2010). In addition, a large number of intermediate-mafic dikes are distributed in the Jiaodong Peninsula (Deng J et al., 2017). Geological structures of different ages, levels, properties, and styles overlap in Jiaodong Peninsula, forming a complex tectonic framework, which shows the mutual superimposition of E-W- and NE-NNE-trending structures overall (Deng J and Wang QF, 2016). The Precambrian tectonic deformation is characterized by folds and ductile shear zones, forming a nearly E-W-trending basement. The Mesozoic tectonic deformation is characterized by brittle faults, which mainly have a NE-NNE strike, followed by nearly E-W and NW-NNW strikes, presenting a NE-NNE-trending fault pattern overall. The large-scale NE-NNE-trending faults include the Sanshandao Fault, Jiaojia Fault, Zhaoping Fault, Xilin-Douya Fault, Mouping-Jimo Fault, and Mouping-Rushan Fault from west to east. These faults control more than 90% of the proven gold resources in the Jiaodong Peninsula (Deng J and Wang QF, 2016; Deng J et al., 2019; Ma YX et al., 2021; Yao XF et al., 2021; Ma XH et al., 2021). The nearly E-W-trending structures mainly include the nearly E-W-trending folds along the axial direction in the Precambrian metamorphic basement and their associated nearly E-W-trending faults, which jointly form an E-W-trending fold-fault belt (Deng J et al., 2019). The NW-NWW-trending structures, with a dip direction of NE or SW, a dip angle of 60°–80°, several to dozens of kilometers long and dozens to hundreds of meters wide, are mainly distributed in the northwestern Jiaodong Peninsula. They are generally post-mineralization faults (Deng J et al., 2019).

3. Ore deposit geology

3.1. General geology

The Dayin'gezhuang gold deposit is located in the central part of the Zhaoping Fault zone (Fig. 2a). The footwall of the Zhaoping Fault zone mainly consists of Upper Jurassic Linglong granites, which contain massive Mesozoic dikes. The hanging wall of the Zhaoping Fault zone is mainly composed of Neoarchean TTG gneisses, with Neoproterozoic Jingshan Group distributed locally. Fault structures are well developed, including the dominant NNE-trending Zhaoping Fault, the NE-trending Houcang and Luanjiahe faults, and the NW-trending Nanzhoujia, Dayin 'gezhuang, and Nangou faults (Fig. 2b).

As a major ore-controlling fault in the Jiaodong Peninsula, the Zhaoping Fault controls the Linglong, Dayin 'gezhuang, Xiadian and Jiudian gold orefields from north to south, with cumulative proven gold reserves of more than 1000 t (Yu XF et al., 2018). This fault has a total length of 120 km, a width of 150–200 m, a dip direction of SE-E, and a dip angle of 30°–70°. In the Dayin 'gezhuang gold deposit, the Zhaoping Fault has an outcrop length of approximately 6.8 km, a strike of 10°–20°, a dip direction of SE, and a dip angle of 10°–58°. This fault has a sharp dip angle in the shallow part, reaching more than 50° locally, and its dip angle gradually decreases to 10°–20° in the deep part. Therefore, the Zhaoping fault is a shovel-shaped fault with a steep upper part and a gentle lower part. The Zhaoping fault has a width of 40–80 m generally and up to 140 m on the surface. It widens toward the depth part, where it has a width of 50–150 m generally and a maximum of greater than 200 m. A continuous and stable major fracture plane has developed in the center part of the Zhaoping Fault and is marked by fault gouges with a thickness of 0.02–2.00 m. The two sides of the major fracture plane consist of cataclastic rocks with different fracture degrees, with early deformed mylonite residues visible locally under the major fracture plane. The Zhaoping Fault shows the characteristics of multiphase activities, including left-lateral transpressional motion before and after the mineralization and right-lateral transtensional motion during the mineralization (Lin WW et al., 2000). Moreover, this fault is cut by the Dayin 'gezhuang and Nanzhoujia faults in the left-lateral direction.

3.2. Alteration types and alteration zones

The wall rocks of the Dayin 'gezhuang gold deposit

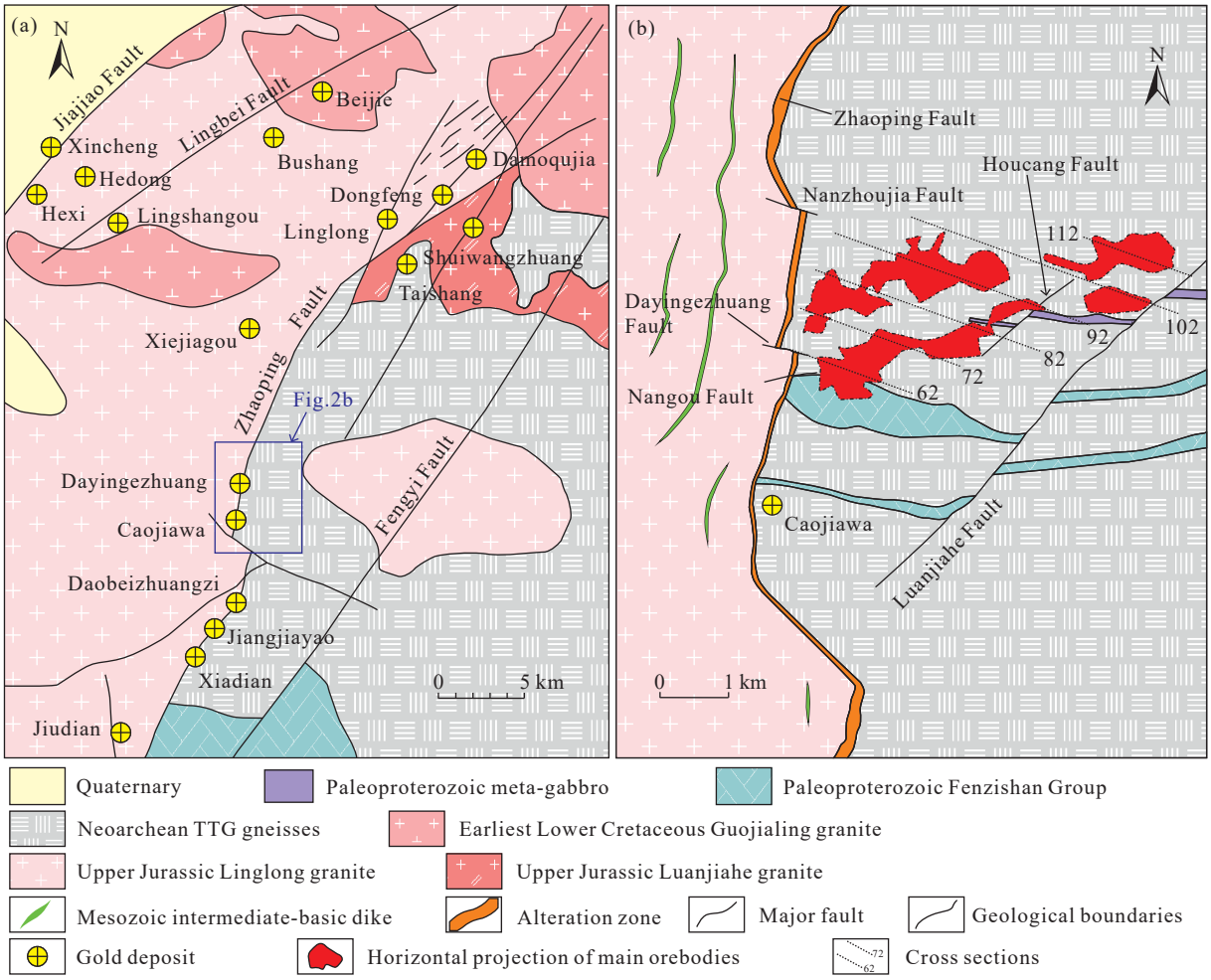

Fig. 2. a–Geological map of the Zhaoping gold belt; b–geological map of the Dayin'gezhuang gold deposit (modified from Liu XD, 2022).

underwent extensive alterations, forming a large alteration zone and complete alteration types, which mainly include K-feldspar alteration, silicification, sericitization, carbonatization, and chloritization (Zhang BL et al., 2017). Moreover, sericitization, silicification, and pyritization occur in combination, forming pyrite-sericite-quartz altered rock.

K-feldspar alteration (Figs. 3b, d) is a type of early hydrothermal alteration and is widely exposed far away from the major fracture plane. It has a width of up to 50–300 m, and its alteration intensity gradually weakens with an increase in the distance from ore-controlling structures. Pyrite-sericite-quartz alteration (Figs. 3a, c, f) is a predominant type of alteration. It is closely related to mineralization and is frequently associated with disseminated fine-grained pyrites, with coarse-grained pyrites occasionally visible. Pyrite-sericite-quartz alteration tends to gradually weaken toward both sides with the major fracture plane as the center and is stronger on the footwall than on the hanging wall. Carbonatization is often interspersed in rocks in the form of veins and stockworks. Carbonatization is more developed on the hanging wall. Chloritization is mainly distributed on the hanging wall and the local fracture plane of the footwall.

The hydrothermal alteration in the Dayin'gezhuang gold deposit shows significant zoning and gradually weakens toward both sides from the major fracture plane. Weak sericitization and chloritization zones are commonly visible on the hanging wall, which features weak alteration and mineralization in general. Therefore, large-scale industrial orebodies rarely occur on the hanging wall. The alteration zones on the footwall include a pyrite-sericite-quartz altered cataclastic rock zone, a pyrite-sericite-quartz altered granitic cataclastic rock zone, a pyrite-sericite-quartz altered granite zone, a normal Linglong granite zone outward from the major fracture plane. These alteration zones gradually transition from one to another (Fig. 4).

3.3. Orebodies and resources

More than 200 gold orebodies have been defined in the Dayin'gezhuang gold deposit. Based on their occurrence locations and geological characteristics, these orebodies can be divided into No. 1 orebodies which are located to the south of the Dayin'gezhuang fault, and No. 2 orebodies which are located to the north of the Dayin'gezhuang fault, respectively (Fig. 2b).

The No. 1 orebodies mainly occur in the shape of irregular large veins in the pyrite-sericite-quartz altered cataclastic rocks on the footwall of the major fracture plane. They are distributed in a gentle wave pattern along their strike and dip

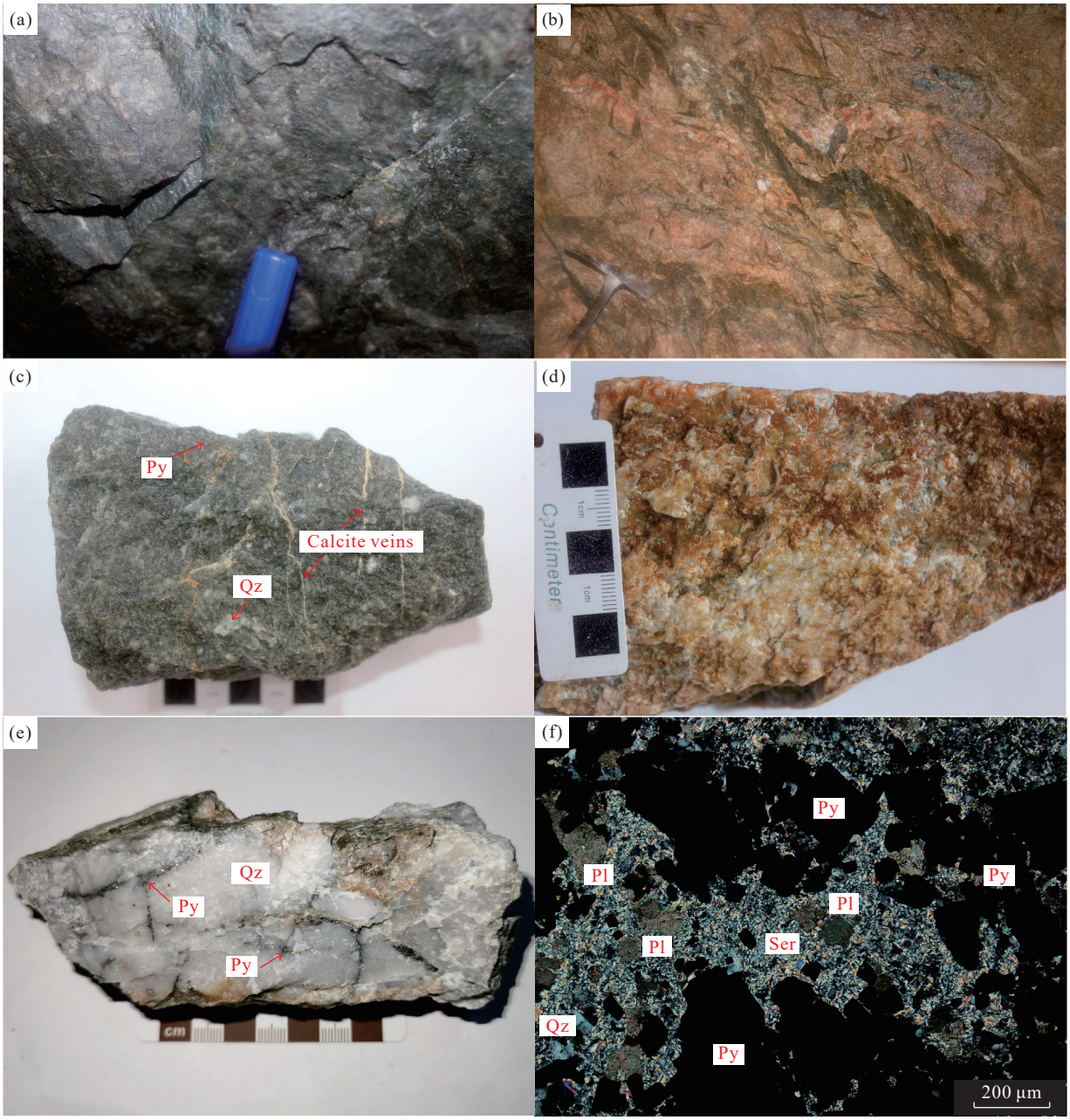

Fig. 3. Photographs (a–e) and photomicrographs (f) of typical hydrothermal alteration in the Dayin'gezhuang gold deposit. a–pyrite-sericite-quartz alteration; b–K-feldspar alteration; c–pyrite-sericite-quartz altered sample cut by calcite veins; d–K-feldspar alteration sample; e–pyrite veins cut silicified sample; f–typical pyrite-sericite-quartz alteration. Pl–plagioclase, Py–pyrite, Qz–quartz, Ser–sericite.

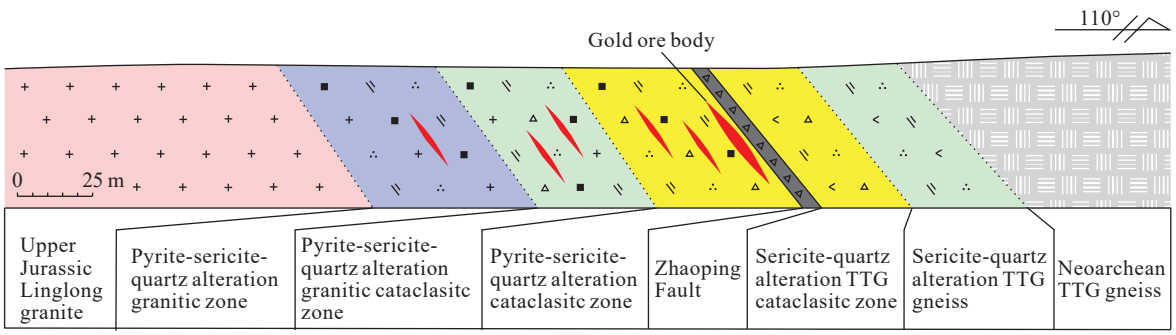

Fig. 4. Comprehensive schematic diagram of lithologic zoning of the hydrothermal alteration zones and fractured zones in the Dayin'gezhuang gold deposit.

direction, with branches and combination as well as swelling and shrinkage (Fig. 5). They have simple morphologies and stable distribution, and have a strike of 2°–30° (average: 20°), a dip direction of SE, and a dip angle of 12°–42° (average: 33°). The occurrence of the orebodies becomes increasingly gentle from shallow to deep. The No. 1 orebodies are located at an elevation of +24 – −1750 m and have a maximum length of 1229 m along their strike and a maximum length of 1236 m along their dip direction. The thickness of single-drilling-controlled orebody is 0.62–20.70 m overall, 2.24–15.90 m in general, and 5.30 m on average. The single-sample gold grade is 1.00–91.50 g/t, with an average of 3.07 g/t.

The No. 2 orebodies mainly occur in the shape of irregular large veins in the pyrite-sericite-quartz altered cataclastic rocks and locally extend into the pyrite-sericite-quartz altered granites on the footwall of the major fracture plane. They are distributed in a gentle wave pattern along their strike and dip direction, with branches and combination as well as swelling

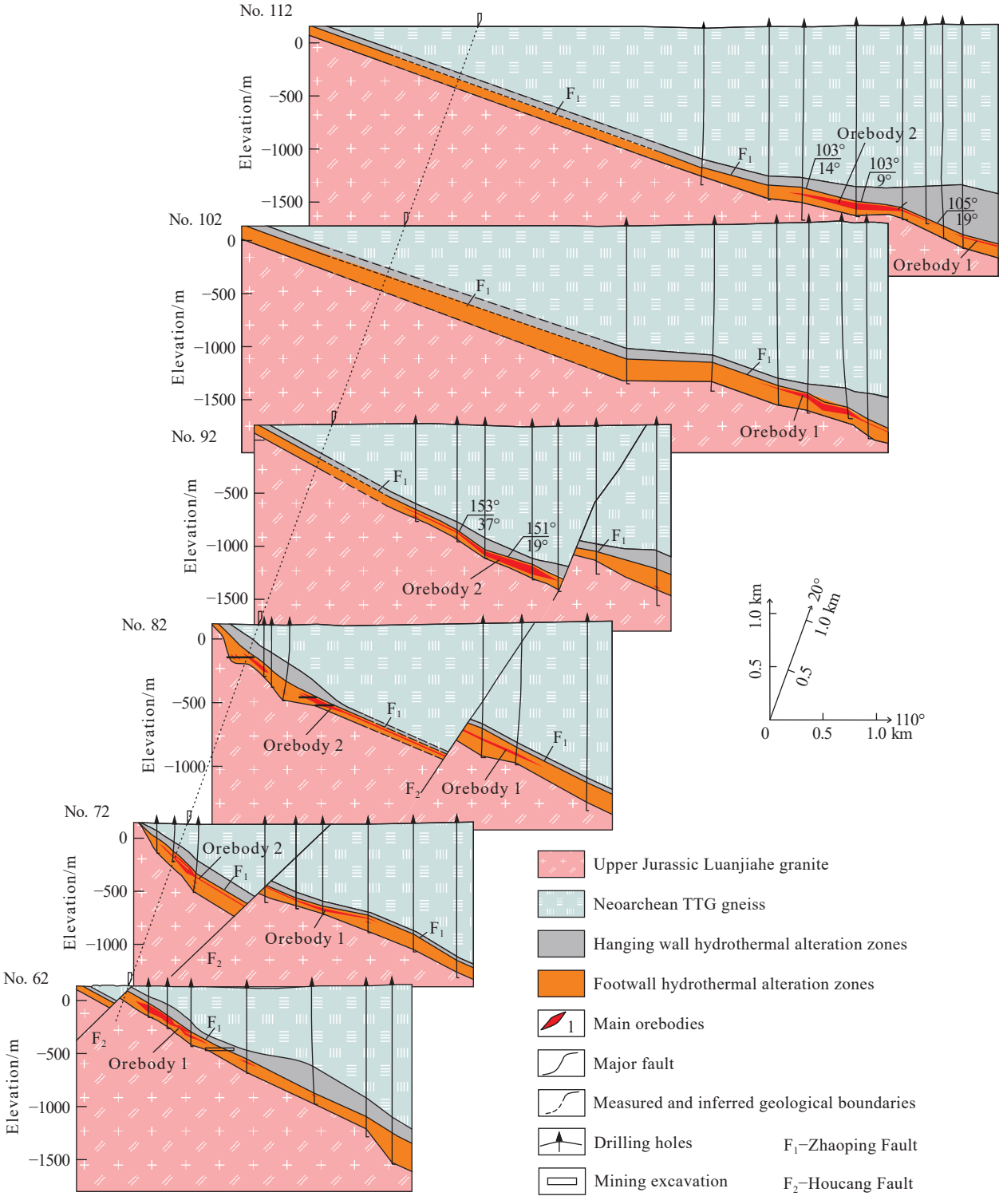

Fig. 5. Combined cross-sections of the Dayin'gezhuang gold deposit.

and shrinkage (Fig. 5). Their attitude are essentially consistent with that of the main fracture plane of the Zhaoping fault, with a strike of 1°–26°, a dip direction of SE, and a dip angle of 18°–51° (average: 39°). The No. 2 orebodies are located at an elevation of −28 – −1933 m and have a maximum length of 1057 m along the strike and a maximum length of 1450 m along the dip direction. The thickness of single-drilling-controlled orebody is 0.64–75.07 m overall, 5.19–40.94 m in general, and 7.16 m on average. The single-sample gold grade is 1.00–66.30 g/t overall, 1.00–4.00 g/t in general, and 3.02 g/t on average.

The orebodies in the Dayin'gezhuang gold deposit have a pitch direction of NNE, a pitch angle of approximately 55°, a plunge direction of NEE 75°, and a plunge angle of approximately 22° overall (Fig. 6).

The shallow (−800–0 m) ore bodies are mainly controlled by tunnels and intensive drilling holes, while the deep (−2000 – −800 m) orebodies are mainly controlled by drilling holes (Fig. 6b). The basic engineering spacing to explore the controlled resources is 120 m × 120 m (strike × dip direction). In fact, the proven resources, controlled resources and inferred resources have been explored in different ore blocks individually, with drilling spacing used including (29–108) m × (38–92) m, (68–129) m × (90–135) m, and (118–244) m × (186 –292) m (strike × dip direction). The cumulative resources of gold ores and gold of all ore blocks are 68×10^6 t and 183 t, respectively, with an average orebody thickness of 9.84 m and an average gold grade of 2.69 g/t. Among them, 43×10^6 t of gold ores and 118 t of gold are obtained from shallow orebodies, with an average orebody thickness of

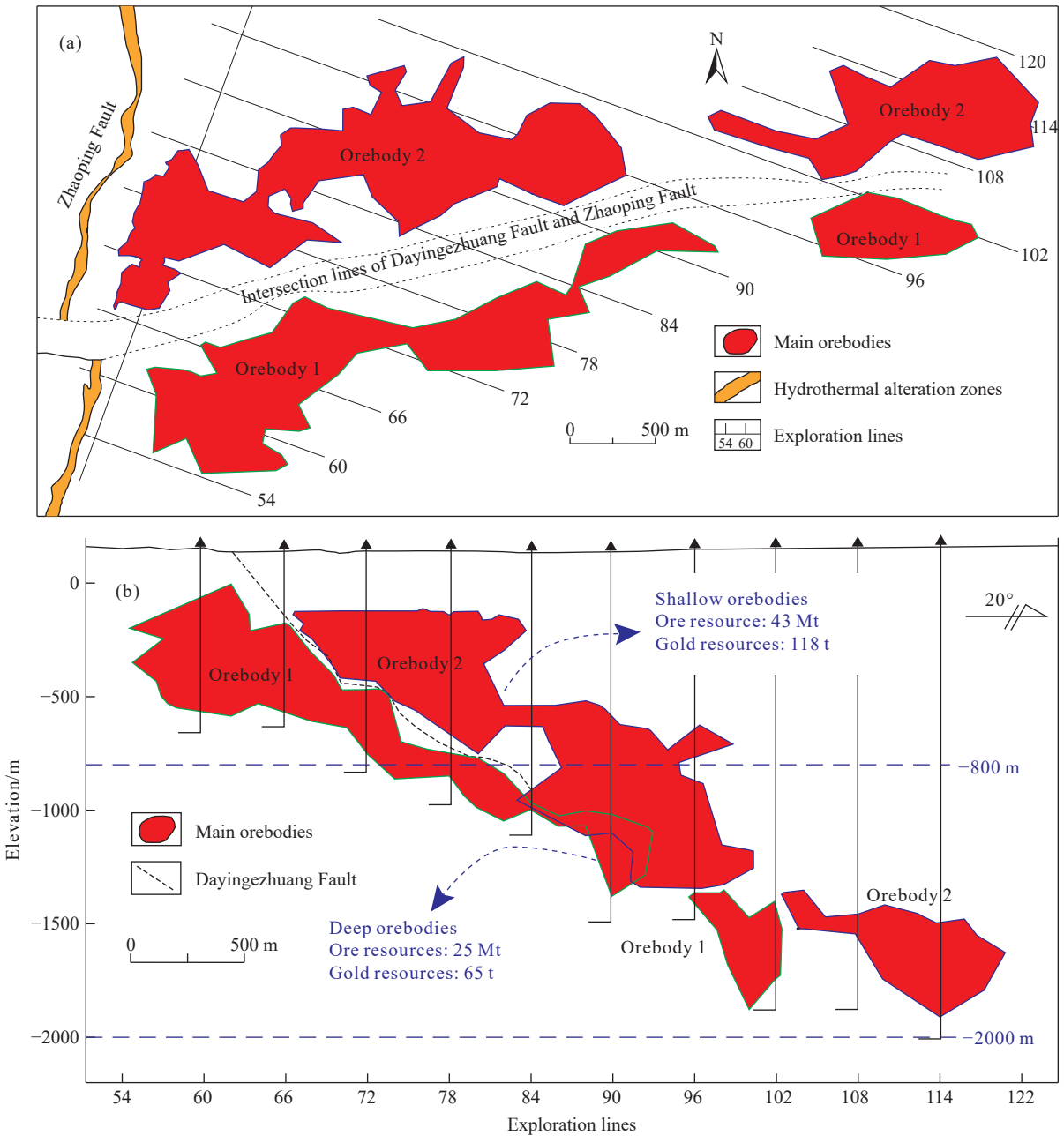

Fig. 6. a–Vertical projection diagram; b–horizontal projection diagram of the main orebodies in the Dayin'gezhuang gold deposit.

10.25 m and an average gold grade of 2.75 g/t. Meanwhile, 25×10^6 t of gold ores and 65 t of gold are obtained from deep orebodies, with an average orebody thickness of 6.15 m and an average gold grade of 2.61 g/t. The gold resources ratio, ore grade ratio, and orebody thickness ratio between deep and shallow orebodies are 0.55, 0.95 and 0.60, respectively. Therefore, the scale and enrichment degree of deep orebodies are both smaller than those of shallow orebodies.es.es.es.

3.4. Ore characteristics

There are mainly three types of ores in the Dayin ' gezhuang gold deposit, namely fine-grained disseminated pyrite-sericite-quartz altered cataclastic rocks (Figs. 7a, b), disseminated and veinlet-stockwork pyrite-sericite-quartz altered granitic cataclastic rocks (Figs. 7c, d), and veinlet-stockwork pyrite-sericite-quartz altered granites (Figs. 7e, f), which are mainly distributed in the pyrite-sericite-quartz altered cataclastic rocks zone, the pyrite-sericite-quartz altered granitic cataclastic rocks zone, and the pyrite-sericite-quartz altered granite zone on the footwall of the major fracture plane respectively. Gold ores are composed of metallic minerals and non-metallic mineral. The primary metal mineral is pyrite, and the secondary ones are chalcopyrite, galena, sphalerite and argentite, whereas non-metallic minerals are dominated by quartz, sericite, K-feldspar and plagioclase, with a small quantity of biotite and calcite (Table 1). Among them, pyrite is the main gold-bearing mineral, followed by quartz. The ore textures are dominated by granular texture, followed by cataclastic, interstitial, etching, poikilitic, and opaque textures. The ore structures are dominated by disseminated and veinlet disseminated structures, followed by spotted, stockwork, and staggered structures.

According to the whole-rock analysis results of seven ore samples (Table 2), the SiO_2 content is high (66.20%–72.64%), with an average of 68.66%. The Al_2O_3 content is 12.24%–14.41%, with an average of 13.72%. The ores also contain a small amount of K_2O (3.82%–5.62%, average 4.73%), Fe_2O_3

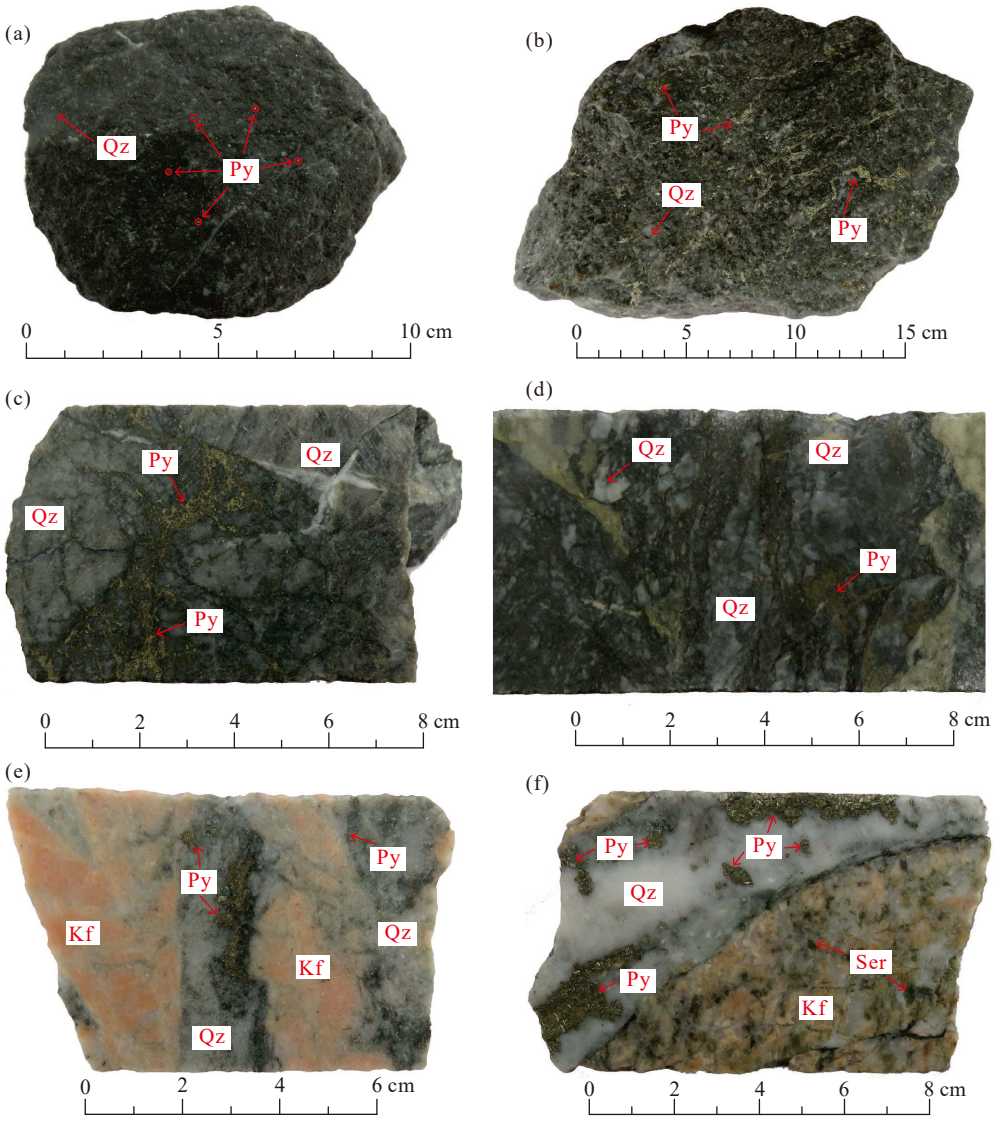

Fig. 7. Main gold ore types in the Dayin'gezhuang gold deposit. a–b–disseminated and veinlet-stockwork pyrite-sericite-quartz alterated cataclastic rock type; c–d–veinlet-stockwork pyrite-sericite-quartz alterated granite cataclastic rock type; e–f–veinlet-stockwork K-feldspar and pyrite-sericite-quartz alterated alteration granite type. Kf–K-feldspar; Py–pyrite; Qz–quartz; Ser–sericite.

Table 1. Mineral composition of ores in the Dayin'gezhuang gold deposit.

Relative content	Metallic minerals			Non-metallic minerals
	Native metals	Sulfides	Others	
Primary	Electrum, Native gold	Pyrite		Quartz, sericite, K-feldspar, plagioclase
Secondary	Native silver, kustelite	Chalcopyrite, galena, sphalerite, argentite	Siderite, limonite	Biotite, calcite
Small amounts	Native bismuth	Pyrrhotite, chalcocite, tetrahedrite, marcasite, covellite, aikinite, galenobismutite, matildite, freibergite, polybasite, antimonpearceite, joseite	Magnetite, specularite, hessite	Chlorite, epidote, orthite, leucoxene, zircon, sphene, apatite, rutile

Table 2. Major elements (%) composition of ores in the Dayin' gezhuang gold deposit.

Sample No.	IQ82-3001	IQ85-3014	IQ85-3015	IQ90-503	IQ90-507	IQ90-513	IQ90-517
SiO_2	69.32	68.58	68.96	67.61	66.2	67.34	72.64
TiO_2	0.16	0.18	0.14	0.16	0.16	0.12	0.11
Fe_2O_3	1.61	3.12	1.42	1.66	3.87	3.01	2.56
FeO	2.22	1.22	1.60	1.36	3.90	4.35	2.90
CaO	3.25	2.11	3.39	3.66	0.30	0.60	0.30
MgO	0.18	0.64	0.52	0.65	1.36	0.81	0.92
P_2O_5	0.05	0.06	0.08	0.05	0.05	0.04	0.03
MnO	0.08	0.08	0.15	0.24	0.82	0.14	0.37
K_2O	5.13	5.62	5.40	4.66	4.22	4.28	3.82
Na_2O	0.13	/	/	0.09	0.12	0.12	0.08
Al_2O_3	13.71	14.12	13.84	14.41	13.94	13.81	12.24
CO_2	2.45	/	/	3.08	2.33	2.57	1.22
H_2O^+	1.82	/	/	2.22	2.83	2.47	2.07
LOI	/	4.40	4.66	/	/	/	/
Total	100.11	100.13	100.16	99.85	100.10	99.66	99.26

Table 3. Trace elements composition of ores in the Dayin' gezhuang gold deposit.

Elements	Au	Ag	S	Cu	Pb	Zn	As
Minimum	1.00	0.01	0.08	0.01	0.01	0.01	0.01
Maximum	91.50	153.54	8.27	0.68	3.91	2.93	0.06
Average	2.58	11.10	1.29	0.05	0.08	0.07	0.02

Note: 10^{-6} for Au and Ag; % for S, Cu, Pb, Zn, and As.

(1.42%–3.87%, average 2.46%), FeO (1.22%–4.35%, average 2.51%), CaO (0.30%–3.66%, average 1.94%), MgO (0.18%–1.36%, average 0.73%). The contents of TiO_2, P_2O_5, MnO and Na_2O are very low.

The primary useful element in the ores is Au, and the associated beneficial elements include Ag, S, Cu, Pb, and Zn, and the hazardous element is As. According to the whole-rock analysis results of 516 ore samples (Table 3), the Au grade ranges from 1.00g/t to 91.50 g/t, with an average of 2.58 g/t. The Ag grade ranges from 0.01 g/t to 153.54 g/t, with an average of 11.10 g/t, which can be used as an associated beneficial component for comprehensive recycling. The contents of other elements such as S, Cu, Pb and Zn are less, not up to the standard of comprehensive utilization. The content of hazardous element As is very low, with an average of 0.02% (0.01%–0.06%).

3.5. Characteristics of gold minerals

The gold minerals in the Dayin'gezhuang gold deposit mainly include electrum (Figs. 8e, f; 68.2%), followed by native gold (31.7%). The fineness of electrum and native gold is 563 –799 (average: 722) and 811 –917 (average: 881), respectively. The gold minerals mainly include fine grains (0.037 –0.01 mm; 39.36%) and micrograins (<0.01 mm; 38.67%) in terms of grain size and are mainly granular (72.32%) in shape. Based on their occurrence states, the gold minerals mainly include the intergranular type (Figs. 8a, c; 60.18%), followed by the fissure type (20.37%) and the inclusion type (Figs. 8b, d; 19.45%).

3.6. Ore-forming stages

The Dayin'gezhuang gold deposit has four ore-forming stages according to mineral assemblages, textures, structures, and the crosscutting relationships of hydrothermal veins (Fig. 9; Yang LQ et al., 2009; Chai P et al., 2019a, 2019b). Stage I is the pyrite-quartz stage. The hydrothermal veins of this stage are white and primarily consisted of quartz and a small number of pyrites and sericites. Stage II is the gold-quartz-pyrite stage. The mineralized veins of this stage are grayish-yellow and distributed as veinlets in fractured zones. They mainly consist of pyrites and a small amount of quartz, sericites, native gold, and electrum. Stage III is the gold-quartz-polymetallic sulfide stage. The mineralized veins of this stage are grayish-yellow and are distributed as veinlets and micro-veins in fractured zones. They mainly consist of quartz, pyrites, chalcopyrite, galena, and sphalerite and a small amount of electrum, kustelite, pyrrhotite, tetrahedrite, galenobismuthite, and native bismuth. Stage IV is the quartz-carbonate stage. The hydrothermal veins of this stage are distributed as veins and veinlets in fractured zones. They mainly consist of calcites and a small amount of quartz.

The mineralization intensity evolved from weak to strong and then weak from early to late ore-forming stages. The mineral assemblages evolved from simple to complex and then simple. They transitioned from only pyrites to the coexisting of galena, sphalerite, pyrites, and finally carbonate veins. Gold was mainly precipitated in ore-forming stages II and III.

4. Ore deposit geochemistry

4.1. Fluid inclusions

The fluid inclusions in the Dayin'gezhuang gold deposit generally have a small diameter of 2 –15 μm and various morphologies, such as the oval, strip, and negative crystal. They mainly have three types, i.e., H_2O-CO_2, H_2O solution,

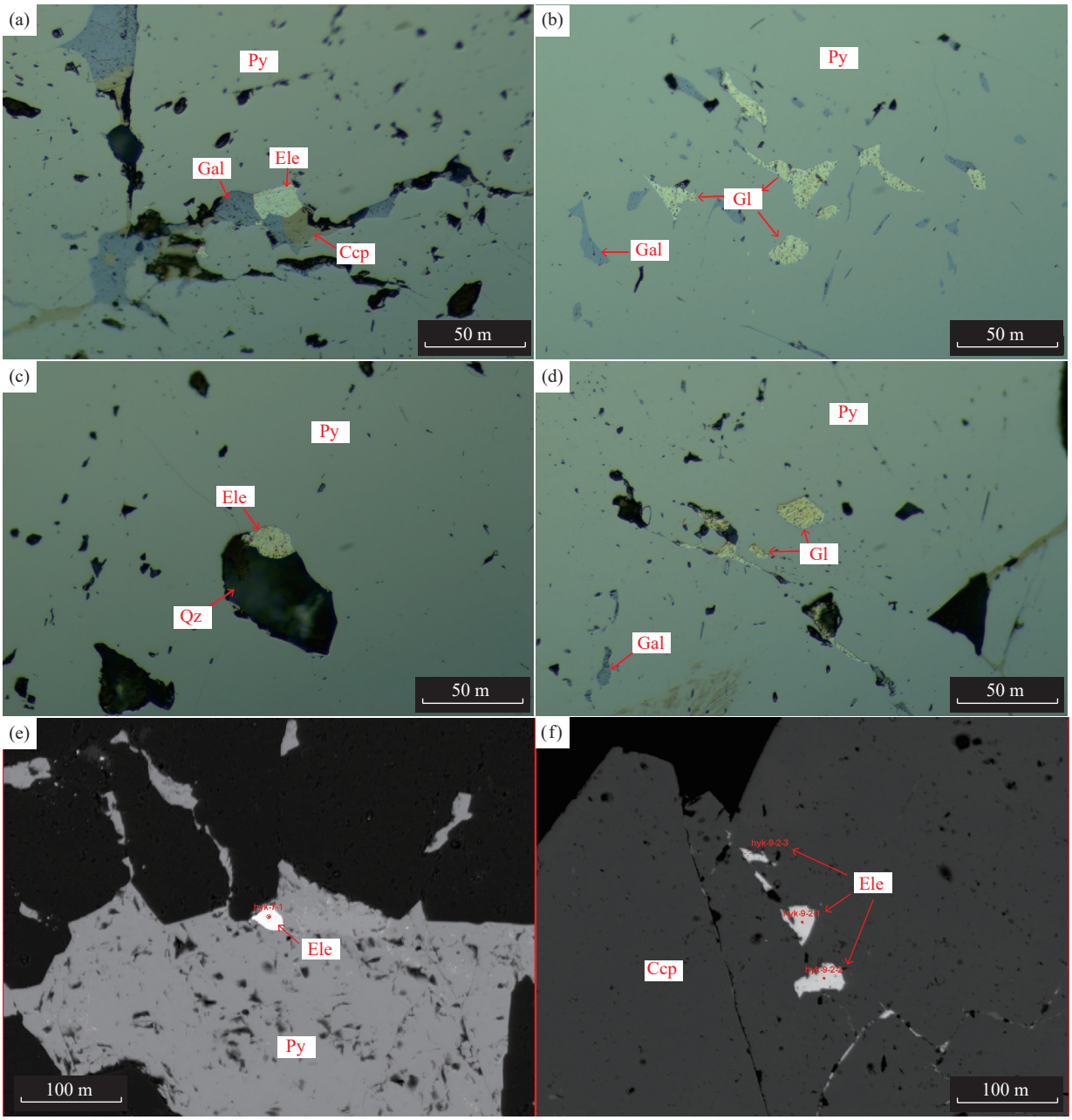

Fig. 8. Photomicrographs (a–d) and backscattered electron images (e, f) of typical gold ores in the Dayin'gezhuang gold deposit. Ccp–chalcopyrite; Ele–electrum; Gal–galena; Gl–native gold; Py–pyrite, Qz–quartz.

and pure CO_2 (Fig. 10). The H_2O-CO_2 inclusions are the most important and are three-phase (L_{H_2O}+L_{CO_2}+V_{CO_2}) or two-phase (L_{H_2O}+L_{CO_2}/V_{CO_2}) at room temperature (25°C). They can be subdivided into H_2O-rich (L_{CO_2}±V_{CO_2}<50%) and CO_2-rich (L_{CO_2}±V_{CO_2}>50%) subtypes according to the proportion of the volume of the CO_2 phases (L_{CO_2}±V_{CO_2}) in the total inclusion volume. The H_2O solution inclusions are two-phase (L_{H_2O}+V_{H_2O}) at room temperature, and their gas-liquid ratio is generally 10%–60%, with a maximum of up to 90%. The pure CO_2 inclusions are two-phase or single-phase (L_{CO_2}±V_{CO_2}) at room temperature.

The vapor-phase components of H_2O-CO_2 inclusions mainly include CO_2 and a small amount of CH_4, C_2H_6, H_2S, SO_2, N_2, and CO, and their liquid-phase components mainly include H_2O (Shen K et al., 2000; Liu Y et al., 2014; Chai P et al., 2019a, 2019b). The pure CO_2 inclusions mainly include CO_2 and a small amount of CH_4 (Chai P et al., 2019a, 2019b). The H_2O solution inclusions are mainly composed of H_2O (Chai P et al., 2019a, 2019b).

The commonly visible inclusions formed at ore-forming stage I include H_2O-CO_2 and pure CO_2 inclusion assemblages. The $T_{m\text{-}CO_2}$ ranges between −58.4°C and −56.6°C, which is slightly lower than the triple point temperature of pure CO_2 (−56.6°C), indicating that the CO_2 phase in the H_2O-CO_2 inclusions may contain a trace amount of CH_4 or other vapor-phase components. The $T_{m\text{-}clath}$ range between 5.3°C and 7.8°C, and $T_{h\text{-}CO_2}$ range is 12.1–30.9°C, and $T_{h\text{-}TOT}$ range is 305–388°C. The salinity ranges from

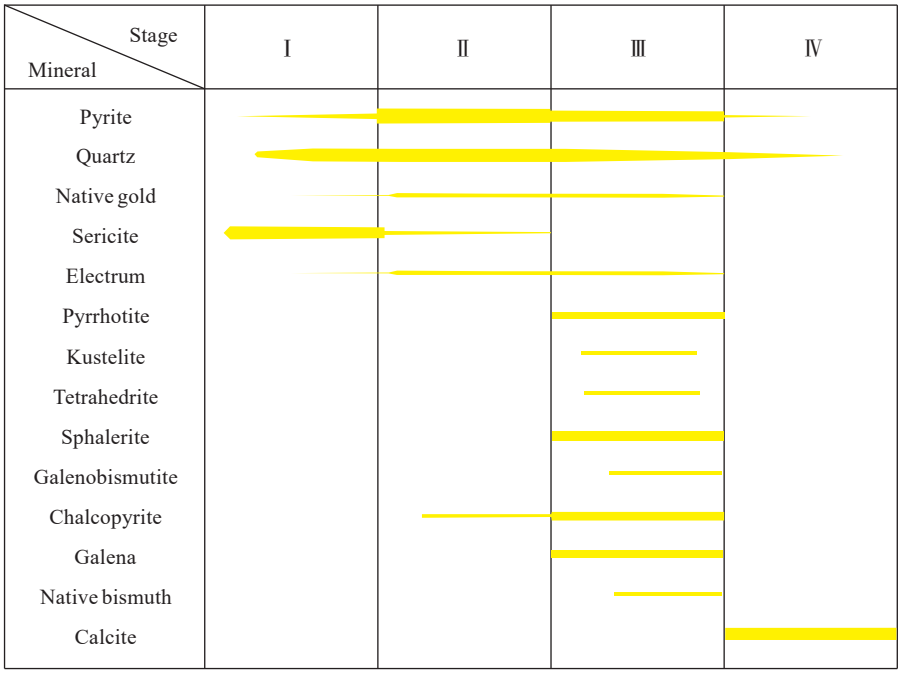

Fig. 9. Paragenetic sequence of main minerals in the Dayin'gezhuang gold deposit (modified from Yang LQ et al., 2009; Chai P et al., 2019a, 2019b).

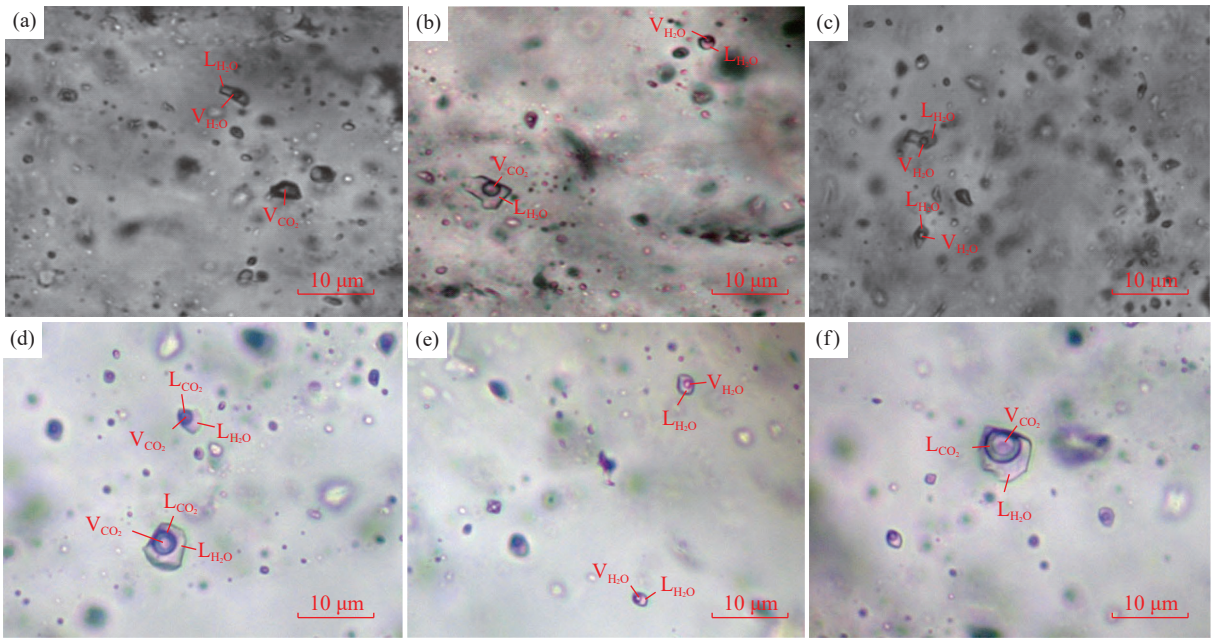

Fig. 10. Photomicrographs of typical fluid inclusions in the Dayin'gezhuang gold deposit. a– aqueous type (H_2O-NaCl) inclusions and pure carbonic type (CO_2) inclusions; b–aqueous type (H_2O-NaCl) inclusions and aqueous-carbonic type (CO_2-H_2O-NaCl) inclusions; c–aqueous type (H_2O-NaCl) inclusions; d–aqueous-carbonic type (CO_2-H_2O-NaCl) inclusions; e–aqueous type (H_2O-NaCl) inclusions; f–aqueous-carbonic type (CO_2-H_2O-NaCl) inclusions.

4.28% NaCl eqv to 8.51% NaCl eqv (Table 4; Fig. 11).

The inclusions formed at ore-forming stage II include the coexisting of H_2O-CO_2, pure CO_2, and H_2O solution inclusions. The $T_{m\text{-}CO_2}$ ranges from −58.1 to −56.6°C, suggesting the CO_2 phase in the H_2O–CO_2 inclusions may contain a trace amount of CH_4 or other vapor-phase components. The $T_{m\text{-}clath}$ is between 6.0 and 8.7°C. The $T_{h\text{-}CO_2}$ ranges between 24.3 and 29.8°C. The $T_{h\text{-}TOT}$ is 235–317°C. The salinity ranges between 2.62% and 7.40% NaCl eqv. The H_2O solution inclusions have a $T_{m\text{-}ice}$ of −7.6 – −0.9°C, a $T_{h\text{-}TOT}$ of 235 –317°C, and salinity of 1.56% –11.12% NaCl eqv (Table 4; Fig. 11).

Similar to stage II, the inclusions formed at ore-forming stage III also include the coexisting of H_2O–CO_2, pure CO_2, and H_2O solution inclusions, except that the proportion of the H_2O solution inclusions increases significantly. The $T_{m\text{-}CO_2}$ ranges from −58.6°C to −56.6°C, suggesting that the CO_2 phase still contains a trace amount of CH_4 or other vapor-

Table 4. Summary of the microthermometric data for fluid inclusions trapped in quartz and calcite from four mineralization stages.

Stage	Fluid inclusion type	$T_{m\text{-}CO_2}$/°C	$T_{m\text{-}cla}$/°C	$T_{h\text{-}CO_2}$/°C	$T_{m\text{-}ice}$/°C	$T_{h\text{-}TOT}$/°C	Salinity/% NaCl eqv	References
Ⅰ	H_2O-CO_2-NaCl	−58.3–−57.1	5.3–7.8	12.1–30.9		305–388	4.28–8.51	Chai P et al., 2019a
Ⅱ	H_2O-CO_2-NaCl	−58.1– −56.6	6.0–8.7	24.3–29.8		235–317	2.62–7.40	
	H_2O-NaCl				−7.6– −0.9	219–301	1.56–11.12	
Ⅲ	H_2O-CO_2-NaCl	−58.6– −56.6	5.9–8.4	21.0–29.8		236–319	3.19–5.09	
	H_2O- NaCl				−9.4– −1.6	195–290	2.73–13.33	
Ⅳ	H_2O- NaCl				−4.2– −1.1	126–233	0.48–6.72	

Note: $T_{m\text{-}CO_2}$, melting temperature of solid CO_2 phase; $T_{m\text{-}cla}$, clathrate melting temperature; $T_{h\text{-}CO_2}$, homogenization temperature of CO_2 phase; $T_{m\text{-}ice}$, temperature of final ice melting; $T_{h\text{-}TOT}$, final homogenization temperature; % NaCl eqv, weight percent NaCl equivalent.

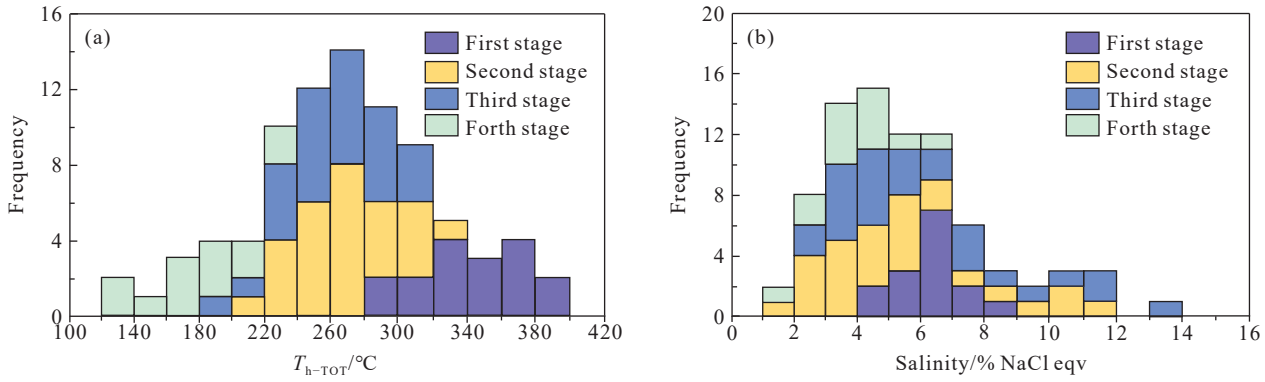

Fig. 11. Histograms of total homogenization temperatures ($T_{h\text{-}TOT}$) and salinities of fluid inclusions in different stages.

phase components. The $T_{m\text{-}clath}$ ranges between 5.9°C and 8.4°C. The $T_{h\text{-}CO_2}$ ranges from 21.0°C to 29.8°C. The $T_{h\text{-}TOT}$ mainly ranges between 236°C and 319°C. The salinity ranges from 3.19% to 7.51% NaCl eqv. For H_2O solution inclusions, the $T_{m\text{-}ice}$ ranges between −9.4°C and −1.6°C. The $T_{h\text{-}TOT}$ ranges from 195°C to 287°C. The salinity ranges from 2.73% to 13.33% NaCl eqv (Table 4; Fig. 11).

The inclusions formed at ore-forming stage IV mainly include H_2O solution inclusions, which have a $T_{m\text{-}ice}$ of −4.2 – −1.1°C, a $T_{h\text{-}TOT}$ of 126 –233°C primarily, and salinity of 0.48%–6.72% NaCl eqv (Table 4; Fig. 11).

4.2. H and O isotopes

The $\delta D_{SMOW\text{-}quartz}$ values range from −99.71‰ to −68.38‰ (average: −77.16‰; n=26) and $\delta^{18}O_{SMOW\text{-}quartz}$ values range from 7.34 ‰ to 12.66 ‰ (average: 10.38 ‰; n=26). The $\delta D_{SMOW\text{-}quartz}$ and $\delta^{18}O_{SMOW\text{-}quartz}$ values of different ore-forming stages are slightly different (Table 5). The hydrothermal quartz of ore-forming stage I has $\delta D_{SMOW\text{-}quartz}$ values of −84.41 ‰ – −68.38 ‰ (average: −75.71 ‰; n=7) and $\delta^{18}O_{SMOW\text{-}quartz}$ values of 7.34‰–12.66‰ (average: 10.55‰; n=7). The hydrothermal quartz of ore-forming stage II has $\delta D_{SMOW\text{-}quartz}$ values of −79.20 ‰ – −69.83 ‰ (average: −73.74‰; n=7) and $\delta^{18}O_{SMOW\text{-}quartz}$ values of 7.34‰–11.81‰ (average: 10.47 ‰; n=7). The hydrothermal quartz of ore-forming stage III has $\delta D_{SMOW\text{-}quartz}$ values of −81.38 ‰ – −70.40‰ (average: −76.07‰; n=6) and $\delta^{18}O_{SMOW\text{-}quartz}$ values of 7.34‰–11.81‰ (average: 10.13‰; n=6). The hydrothermal quartz of ore-forming stage IV has the $\delta D_{SMOW\text{-}quartz}$ values of −99.71 ‰ – −78.71 ‰ (average: −83.93 ‰; n=6) and $\delta^{18}O_{SMOW\text{-}quartz}$ values of 7.34‰ –11.81‰ (average: 10.31‰; n=6).

The hydrogen isotope value of hydrothermal quartz ($\delta D_{SMOW\text{-}quartz}$) represents the hydrogen isotope value of fluid ($\delta D_{SMOW\text{-}water}$), but the oxygen isotope value of fluid ($\delta^{18}O_{SMOW\text{-}water}$) should be calculated based on the oxygen isotope values of hydrothermal quartz ($\delta^{18}O_{SMOW\text{-}quartz}$) and the corresponding metallogenic temperatures of different ore-forming stages. The calculation equations (Clayton RN et al., 1972) are as follows:

$$10^3 \ln\alpha_{quartz\text{-}water}=3.38\times10^6 T^{-2}-3.40;$$

$$\ln\alpha_{quartz\text{-}water}=(1000+\delta^{18}O_{SMOW\text{-}quartz})/(1000+\delta^{18}O_{SMOW\text{-}water}).$$

In general, the total homogenization temperature of fluid inclusions represents the lower limit of the trapping temperature. However, significant fluid immiscibility occurred in ore-forming stages II and III of the Dayin ' gezhuang gold deposit. Therefore, the total homogenization temperature of fluid inclusions can approximately represent the metallogenic temperature (Hagemann SG and Lüders V, 2003). Based on the microthermometry of the abovementioned fluid inclusions, the metallogenic temperatures of the Dayin 'gezhuang gold deposit at ore-forming stages I–IV were 340°C, 280°C, 250°C, and 200°C, respectively.

As indicated by the calculation results (Table 5), the ore-forming fluids in the Dayin 'gezhuang gold deposit have $\delta D_{SMOW\text{-}water}$ values of −99.71 ‰ – −68.38 ‰ (average: −77.16‰; n=26) and $\delta^{18}O_{SMOW\text{-}water}$ values of −4.36‰–7.07‰ (average: 2.05 ‰; n=26). The ore-forming fluids of ore-

Table 5. Hydrogen and oxygen isotope compositions from four ore-forming stages in the Dayin'gezhuang gold deposit.

Sample	Lithology	Stage	Mineral	δD_{SMOW}/‰	$\delta^{18}O_{SMOW}$/‰	$\delta^{18}O_{H2O}$/‰	References
Dygz4	Ore	/	Sericite	−64	9.3	6.98	Mao JW et al., 2005
Dygz5	Ore	/	Sericite	−58	9.5	7.18	
Dygz7	Ore	/	Sericite	−52	8.8	6.48	
Dygz8	Ore	/	Sericite	−58	9.2	6.88	
Dygz9	Ore	/	Sericite	−60	9.3	6.98	
Y62-210B	Quartz-pyrite vein	I	Quartz	−84.41	12.66	7.07	Wei YJ et al., 2020
Y62-290C-1	Quartz vein	I	Quartz	−70.25	11.81	6.22	
Y75-247-5A-1	Silicified and K-feldspar altered cataclastic rock-type ore	I	Quartz	−72.83	10.78	5.19	
Y61-210-4B-1	Silicified and K-feldspar altered cataclastic granite	I	Quartz	−83.25	9.59	4.00	
Y75-247-6A-1	Pyritization and K-feldspar altered granite	I	Quartz	−68.38	7.34	1.75	
/	Quartz vein	I	Quartz	−78.00	10.90	5.31	Zhang LG et al., 1994
0911	Quartz-pyrite vein	I	Quartz	−72.83	10.78	5.19	Dai XL, 2012
Y62-290C-2	Quartz vein	II	Quartz	−70.43	11.81	4.16	Wei YJ et al., 2020
Y75-247-5A-2	Silicified and K-feldspar altered cataclastic rock-type ore	II	Quartz	−70.04	10.78	3.13	
Y61-210-4B-2	Silicified and K-feldspar altered cataclastic granite	II	Quartz	−78.56	9.59	1.94	
Y75-247-6A-2	Pyritization and K-feldspar altered granite	II	Quartz	−70.15	7.34	−0.31	
/	Quartz-base metals vein	II	Quartz	−78.00	11.30	3.65	Zhang LG et al., 1994
Y309Cc-2	Quartz-pyrite vein	II	Quartz	−69.83	11.59	3.94	Wei YJ et al., 2020
0919	Silicified and K-feldspar altered cataclastic rock	II	Quartz	−79.20	10.91	3.26	Dai XL, 2012
Y62-290C-3	Quartz vein	III	Quartz	−74.58	11.81	2.86	①
Y75-247-5A-3	Silicified and K-feldspar altered cataclastic rock type ore	III	Quartz	−78.71	10.78	1.83	Wei YJ et al., 2020
Y61-210-4B-3	Silicified and K-feldspar altered cataclastic granite	III	Quartz	−81.38	9.59	0.64	
Y75-247-6A-3	Pyritization and K-feldspar altered granite	III	Quartz	−79.29	7.34	−1.61	
Y309Cc-3	Quartz-pyrite vein	III	Quartz	−72.04	11.59	2.64	
0928	Pyrite-sericite-quartz alteration cataclastic rock	III	Quartz	−70.40	9.67	0.72	Dai XL, 2012
Y62-290C-4	Quartz vein	IV	Quartz	−78.81	11.81	0.11	①
Y75-247-5A-4	Silicified and K-feldspar altered cataclastic rock-type ore	IV	Quartz	−81.26	10.78	−0.92	
Y61-210-4B-4	Silicified and K-feldspar altered cataclastic granite	IV	Quartz	−82.42	9.59	−2.11	
Y75-247-6A-4	Pyritization and K-feldspar altered granite	IV	Quartz	−99.71	7.34	−4.36	
Y309Cc-4	Quartz-pyrite vein	IV	Quartz	−82.69	11.59	−0.11	
0936	Quartz-carbonate vein	IV	Quartz	−78.71	10.75	−0.95	Dai XL, 2012

Note: ① China University of Geosciences (Beijing), 2005. Study on the overlapping of multiple structural systems and mineralization network of the Dayin' gezhuang gold deposit, Zhaoyuan city, Shandong Province.

forming stage I have $\delta D_{SMOW\text{-}water}$ values of −84.41 ‰ – −68.38‰ (average: −75.71‰; n=7) and $\delta^{18}O_{SMOW\text{-}water}$ values of 1.75‰–7.07‰ (average: 4.96‰; n=7). The ore-forming fluids of ore-forming stage II have $\delta D_{SMOW\text{-}water}$ values of −79.20 ‰ – −69.83 ‰ (average: −73.74 ‰; n=7) and $\delta^{18}O_{SMOW\text{-}water}$ values of −0.31‰–4.16‰ (average: 2.83‰; n=7). The ore-forming fluids of ore-forming stage III have $\delta D_{SMOW\text{-}water}$ values of −81.38 ‰ – −70.40 ‰ (average: −76.07‰; n=6) and $\delta^{18}O_{SMOW\text{-}water}$ values of −1.61‰–2.86‰ (average: 1.18‰; n=6). The ore-forming fluids of ore-forming stage IV have $\delta D_{SMOW\text{-}water}$ values of −99.71‰ – −78.71‰ (average: −83.93 ‰; n=6) and $\delta^{18}O_{SMOW\text{-}water}$ values of −4.36‰–0.11‰ (average: −1.39‰; n=6).

The hydrothermal sericites of ore-forming stages II and III in the Dayin 'gezhuang gold deposit have $\delta D_{SMOW\text{-}sericite}$ values of −64‰ – −52‰ (Table 2; average: −58‰; n=5) and $\delta^{18}O_{SMOW\text{-}sericite}$ values of 8.8‰–9.5‰ (average: 9.2‰; n=5). The hydrogen isotope value of hydrothermal sericites ($\delta D_{SMOW\text{-}sericite}$) represents the hydrogen isotope value of fluids ($\delta D_{SMOW\text{-}water}$). But the oxygen isotope value of fluids ($\delta^{18}O_{SMOW\text{-}water}$) should be calculated according to the oxygen isotope values of hydrothermal sericites ($\delta^{18}O_{SMOW\text{-}sericite}$) and

the corresponding metallogenic temperatures at different ore-forming stages. The calculation equations (Zheng YF and Chen JF, 2000) are as follows:

$10^3\ln\alpha_{phengite\text{-}water}=4.13\times10^6/T^2-7.41\times10^3/T+2.20$;

$\ln\alpha_{phengite\text{-}water}=(1000+\delta^{18}O_{SMOW\text{-}phengite})/(1000+\delta^{18}O_{SMOW\text{-}water})$ (0–1200°C).

According to the calculation results, the $\delta D_{SMOW\text{-}water}$ and $\delta^{18}O_{SMOW\text{-}water}$ values of ore-forming stages II and III are −64‰ – −52‰ (average: −58‰; n=5) and 6.48‰–7.18‰ (average: 6.90‰; n=5), respectively.

4.3. S isotopes

The Dayin 'gezhuang gold deposit has $\delta^{34}S_{CDT}$ values

Table 6. Sulfur isotope compositions from four ore-forming stages in the Dayingezhuang gold deposit.

Sample	Lithology	Stage	Mineral	$\delta^{34}S$	References
Dygz3	Ore	/	Pyrite	7.60	Mao JW et al., 2005
Dygz4	Ore	/	Pyrite	7.90	
Dygz7	Ore	/	Pyrite	7.50	
Dygz8	Ore	/	Pyrite	7.50	
Dygz9	Ore	/	Pyrite	7.20	
Dygz6	Ore	/	Pyrite	7.80	
Dygz10	Ore	/	Pyrite	6.80	
IS81-3001	Coarse veined ore	I	Pyrite	7.20	①
IS82-3003	Coarse veined ore	I	Pyrite	7.28	
Y61-210-1A	Sericite-quartz altered rock	I	Pyrite	7.18	Zhang RZ et al., 2016
Y61-210-1B	Sericite-quartz altered rock	I	Pyrite	7.21	
Y61-210-5B	Silicified and K-feldspar altered granite	I	Pyrite	7.48	
Y75-247-1A	Pyrite-sericite-quartz altered rock	I	Pyrite	7.41	
Y75-247-2A	Quartz-base metals vein	I	Pyrite	7.54	
Y61-210-2B	Pyrite-sericite-quartz altered rock	I	Pyrite	7.28	
Y62-210A	Quartz-pyrite vein	I	Pyrite	7.22	
Y62-210B	Quartz-pyrite vein	I	Pyrite	7.26	
0911	Quartz-pyrite vein	I	Pyrite	7.32	Dai XL, 2012
DYG33-1	Disseminated and stockwork ore	I	Pyrite	9.0	Yuan ZZ et al., 2019
DYG33-2	Disseminated and stockwork ore	I	Pyrite	8.3	
DYG-52	Disseminated and stockwork ore	I	Pyrite	5.8	
DYG36-1	Disseminated and stockwork ore	I	Pyrite	7.1	
DYG36-2	Disseminated and stockwork ore	I	Pyrite	7.6	
DYG11-1	Disseminated and stockwork ore	I	Pyrite	8.0	
DYG11-2	Disseminated and stockwork ore	I	Pyrite	8.2	
DYG11-3	Disseminated and stockwork ore	I	Pyrite	7.1	
DYG23-1	Disseminated and stockwork ore	I	Pyrite	7.5	
DYG23-2	Disseminated and stockwork ore	I	Pyrite	7.8	
1Da90-502	Ore	II	Pyrite	5.50	①
IS81-3002	Fine-grained vein ores	II	Pyrite	5.90	
IS82-3001	Fine-grained vein ores	II	Pyrite	7.40	
IS82-3002	Fine-grained vein ores	II	Pyrite	6.75	
Y61-210-4B	Silicified and K-feldspar altered cataclastic granite	II	Pyrite	6.78	Zhang RZ et al., 2016
Y61-290-1	Pyrite-sericite-quartz altered rock	II	Pyrite	6.92	
Y75-247-5A	Silicified and K-feldspar altered cataclastic rock type ore	II	Pyrite	7.11	
Y75-247-6A	Pyritization and K-feldspar altered granite	II	Pyrite	6.84	
0919	Pyritization and silicified altered cataclastic rock	II	Pyrite	5.61	Dai XL., 2012
DYG32-1	Disseminated and stockwork ore	II	Pyrite	5.3	Yuan ZZ et al., 2019
DYG32-2	Disseminated and stockwork ore	II	Pyrite	7.1	
DYG38-1	Disseminated and stockwork ore	II	Pyrite	7.7	
DYG38-2	Disseminated and stockwork ore	II	Pyrite	7.4	
DYG43-1	Disseminated and stockwork ore	II	Pyrite	6.5	
DYG43-2	Disseminated and stockwork ore	II	Pyrite	5.4	
DYG44	Disseminated and stockwork ore	II	Pyrite	4.8	
DYG7-1	Disseminated and stockwork ore	II	Pyrite	5.2	
DYG7-2	Disseminated and stockwork ore	II	Pyrite	8.0	
DYG8-1	Disseminated and stockwork ore	II	Pyrite	8.0	
DYG8-2	Disseminated and stockwork ore	II	Pyrite	7.8	

Table 6. (*Continued*)

Sample	Lithology	Stage	Mineral	$\delta^{34}S$	References
IS82-3004	Coarse veined ore	Ⅲ	Sphalerite	7.29	①
IS82-3005	Sericite-quartz altered rock	Ⅲ	Chalcopyrite- Pyrite	6.75	
Y62-290C	Quartz vein	Ⅲ	Pyrite	6.57	Zhang RZ et al., 2016
Y61-290-4	Quartz-base metals vein	Ⅲ	Pyrite	6.82	
Y79-356K	Quartz-base metals vein	Ⅲ	Sphalerite	6.86	
Y79-356K	Quartz-base metals vein	Ⅲ	Galena	4.99	
0928	Disseminated and stockwork ore	Ⅲ	Pyrite	5.91	Dai XL, 2012
DYG39-1	Disseminated and stockwork ore	Ⅲ	Pyrite	6.9	Yuan ZZ et al., 2019
DYG39-2	Disseminated and stockwork ore	Ⅲ	Pyrite	6.4	
DYG57	Disseminated and stockwork ore	Ⅲ	Pyrite	6.2	
DYG59	Disseminated and stockwork ore	Ⅲ	Pyrite	7.6	
DYG22-1	Disseminated and stockwork ore	Ⅲ	Pyrite	6.4	
DYG22-2	Disseminated and stockwork ore	Ⅲ	Pyrite	7.2	
DYG22-3	Disseminated and stockwork ore	Ⅲ	Pyrite	6.7	
Y55-210Ka	Silver-polymetallic sulphide ore	Ⅳ	Galena	4.61	Zhang RZ et al., 2016
Y55-210Kb	Silver-polymetallic sulphide ore	Ⅳ	Galena	4.58	
Y309-Cc	Quartz-carbonate vein	Ⅳ	Pyrite	6.98	
0936	Quartz-carbonate vein	Ⅳ	Pyrite	6.73	Dai XL, 2012

Note: ① Shandong Provincial No.6 Exploration Institute of Geology and Mineral Resources, 1992. Intermediate geological report on the exploration of Taishang gold deposit in Zhaoyuan City, Shandong Province.

(Table 6) of 4.6‰–9.0‰, with a range of 4.4‰ and an average of 6.9‰ (n=66). Specifically, the $\delta^{34}S_{CDT}$ values of ore-forming stage I are 5.8‰–9.0‰, with a range of 3.2‰ and an average of 7.5‰ (n=21); those of ore-forming stage II are 4.8‰–8.0‰, with a range of 3.2‰ and an average of 6.6‰ (n=20), those of ore-forming stage III are 5.0‰–7.6‰, with a range of 2.6‰ and an average of 6.6‰ (n=14), and those of the ore-forming stage IV are 4.6‰–7.0‰, with a range of 2.4‰ and an average of 5.7‰ (n= 4).

4.4. Pb isotopes

The Pb isotopes of the Dayin'gezhuang gold deposit vary in a small range and have a relatively stable composition (Table 7). The $^{206}Pb/^{204}Pb$ values are 17.1100–17.3585, with an average of 17.2731 (n=42), the $^{207}Pb/^{204}Pb$ values are 15.4000–15.6116, with an average of 15.4815 (n=42), and the $^{208}Pb/^{204}Pb$ values are 37.6000–38.3328, with an average of 37.9180 (n=42).

5. Discussion

5.1. Spatial coupling relationships between ore-controlling fault and orebodies

To analyze the deep occurrence characteristics of the ore-controlling Zhaoping Fault and the spatial coupling relationship between the fault and orebodies in detail, a three-dimensional geological model of the Dayin'gezhuang gold deposit at an elevation of −2000–0 m was established based on drilling holes data and the data on exploration lines. Then, the fault slope is plotted using the information about the major fracture plane of the Zhaoping Fault extracted from the model (Fig. 12; Xie TC et al., 2022). As shown in the diagram, the dip angle of the fault is high in the shallow and gradually decreases towards the deep at an elevation of −2000–0 m. Moreover, the fault surface undulates significantly and presents a shovel-shaped stepped pattern overall. This plot also shows that there are three NNE-trending zones with a high dip angle (in red), between and besides which are zones with a low dip angle (in yellow and green), indicating that the fault dip angle presents three sections of stepped high-to-low transitions. The stepped characteristic of this fault is similar to that of the Sanshandao and Jiaojia faults, indicating that these three major ore-controlling faults (Sanshandao, Jiaojia, and Zhaoping faults) in the Jiaodong Peninsula have consistent morphological characteristics (Song MC et al., 2012, 2021b). Therefore, they should belong to the same fault system formed under a unified dynamic setting and are detachment faults developing between Precambrian metamorphic rocks and Jurassic granites (Song MC et al., 2022a).

To analyze the occurrence characteristics of the gold orebodies, the gold orebodies damaged by the Dayin'gezhuang and Houcang faults are restored and the thickness × grade distribution map of major orebodies is plotted. As shown in the map, there are multiple mineralization enrichment areas with high thickness × grade values. These mineralization enrichment areas are distributed in a beaded pattern along the dip directions of the orebodies, roughly forming two near-parallel bead zones in the south and the north each. The general distribution direction of the bead zones indicates that the orebodies have a plunge direction of 75°. The mineralization enrichment areas are present as NNE-trending zones and show an alternating distribution with weakly mineralized zones (Fig. 13).

The map showing the main orebodies distribution and mineralization enrichment areas and the diagram presenting

Table 7. Lead isotopic compositions of the Dayin'gezhuang gold deposit.

Sample	Mineral	$^{206}Pb/^{204}Pb$	$^{207}Pb/^{204}Pb$	$^{208}Pb/^{204}Pb$	References
IDa90-505	Galena	17.2950	15.5130	38.0130	①
147	Pyrite	17.1100	15.4400	37.6700	Xu B, 1999
177	Pyrite	17.1600	15.4000	37.6000	
Y55-210K	Galena	17.2638	15.4663	37.8580	Zhang L et al., 2014
Y61-210-1B	Pyrite	17.3102	15.5010	37.9775	
Y61-210-2B	Pyrite	17.2914	15.4901	37.9704	
Y61-210-3B	Pyrite	17.3153	15.5023	37.9818	
Y61-290-1	Pyrite	17.2669	15.5176	38.0333	
Y61-290-4	Pyrite	17.3585	15.6116	38.3328	
Y62-210A	Pyrite	17.3187	15.5412	38.1201	
Y62-210B	Pyrite	17.2840	15.4946	37.9539	
Y62-290C	Pyrite	17.2853	15.5053	37.9899	
Y75-247-1A	Pyrite	17.2301	15.4773	37.8900	
Y75-247-4A	Pyrite	17.3286	15.5084	38.0004	
Y75-247-5A	Pyrite	17.2756	15.4965	37.9157	
Y75-247-6A	Pyrite	17.2949	15.4819	37.9441	
Y79-356K	Sphalerite	17.2359	15.4860	37.9198	
Y79-356K	Galena	17.2157	15.4595	37.8306	
DYG33-1	Pyrite	17.336	15.504	37.9840	Yuan ZZ et al., 2019
DYG33-2	Pyrite	17.182	15.414	37.7290	
DYG36-1	Pyrite	17.326	15.481	37.9480	
DYG36-2	Pyrite	17.330	15.486	37.9700	
DYG11-1	Pyrite	17.234	15.468	37.8740	
DYG11-2	Pyrite	17.241	15.472	37.9530	
DYG23	Pyrite	17.241	15.473	37.8840	
DYG32	Pyrite	17.299	15.464	37.9000	
DYG38-1	Pyrite	17.249	15.43	37.8660	
DYG38-2	Pyrite	17.308	15.486	37.9400	
DYG43-1	Pyrite	17.289	15.465	37.9050	
DYG43-2	Pyrite	17.317	15.486	37.9630	
DYG44	Pyrite	17.308	15.479	37.9150	
DYG45	Pyrite	17.335	15.492	37.9680	
DYG7-1	Pyrite	17.256	15.469	37.8850	
DYG7-2	Pyrite	17.251	15.467	37.8730	
DYG8-1	Pyrite	17.292	15.476	37.9180	
DYG8-2	Pyrite	17.328	15.493	37.9680	
DYG39-1	Pyrite	17.339	15.489	37.9710	
DYG57-1	Pyrite	17.279	15.485	37.7470	
DYG59-1	Pyrite	17.278	15.484	37.8310	
DYG22-1	Pyrite	17.207	15.459	37.8670	
DYG22-2	Pyrite	17.226	15.476	37.8870	
DYG22-3	Pyrite	17.181	15.431	37.8100	

Note: ① China University of Geosciences (Beijing), 2005. Study on the overlapping of multiple structural systems and mineralization network of the Dayin' gezhuang gold deposit, Zhaoyuan city, Shandong Province.

the slope of the major fracture plane of the Zhaoping Fault are superimposed together, showing that the locations of mineralization enrichment areas are basically consistent with the steep-to-gentle transition parts of the fault surface's slope and mainly occur at positions with a gentle fault dip angle (Fig. 12). This result indicates that the gold mineralization enrichment areas are mainly distributed in the transition parts of the fault dip angle and relatively gentle steps, forming a stepped pattern from shallow to deep.

The above-mentioned pitch and plunge regularity and stepped pattern of orebodies are widely distributed in the Jiaodong area (Song MC et al., 2012, 2020b, 2022b; Li SY et al., 2022). The formation of the stepped pattern is related to the change in fluid pressure affected by the change in the fault dip angle. When fluids flew through the steep-to-gentle transition sections of a fault and migrated toward gently dipping sections, the pressure suddenly decreased, and the fluids began to flow in a nearly horizontal direction at a low flow velocity. All these created favorable conditions for fluid unloading and gold precipitation. The fault transitions along its strike and dip direction jointly control the pitch and plunge direction of gold orebodies (Song MC et al., 2022a). The

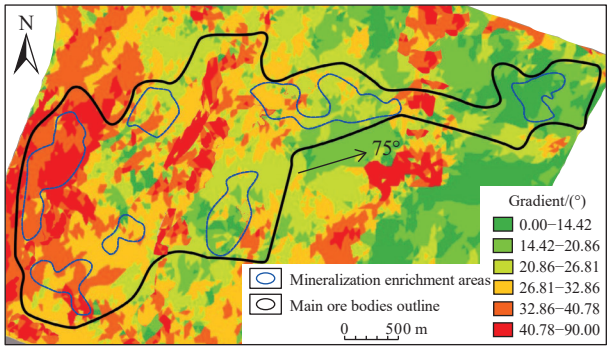

Fig. 12. Diagram showing the relationships between the fault dip angle and the mineralization enrichment areas of main orebodies along with the fault dip direction in the Dayin'gezhuang gold deposit (modified from Xie TC et al., 2022).

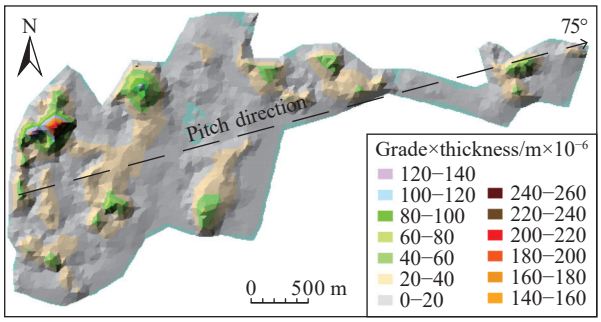

Fig. 13. Three-dimensional distribution maps of the thickness × gold grade of main orebodies in the Dayin'gezhuang gold deposit (modified from Xie TC et al., 2022).

stepped pattern and the pitch and plunge regularities of orebodies play an important role in deep orebodies prospecting. These occurrence patterns of gold orebodies have been applied to the deep orebodies prospecting of the Dayin' gezhuang gold deposit and the Sanshandao, Jiaojia, and Taishang-Shuiwangzhuang supergiant gold deposits.

5.2. Metallogenic epoch

The metallogenic age of the Jiaodong gold deposits has been determined to be 120±2 Ma (Deng J et al., 2020c; Zhang L et al., 2020). According to the testing results (Table 8) of the isotopic age of hydrothermal minerals in the Dayin ' gezhuang gold deposit, the K-feldspars and sericites/muscovites have $^{40}Ar/^{39}Ar$ ages of 118±1 Ma and (119.1±1.2)–(133.37±0.56) Ma, respectively. Different researchers provided different explanations for the metallogenic time of the gold deposit based on these results. Yang LQ et al. (2014a) believed that metallogenic events in the Dayin'gezhuang gold deposit occurred at 134 –126 Ma. Yuan ZZ et al. (2019) determined the ^{40}Ar-^{39}Ar age of sericites to be 119.1±1.2 Ma and the zircon U-Pb age of mafic dikes before metallogenic events to be 122.7±2.6 Ma. Therefore, they considered that the Dayin 'gezhuang gold deposit had a metallogenic age of 119.1±1.2 Ma. Charles N et al (2013) determined the $^{40}Ar/^{39}Ar$ plateau age of muscovites in Linglong granites on the footwall of the Zhaoping fault to be 133.98±1.47 Ma. They believed that this age resulted from the early ductile deformation of the Linglong detachment fault (the southern segment of the Zhaoping fault) and that the ductile and brittle deformation of the Linglong detachment fault lasted from 143 Ma to 128 Ma. Based on the above studies, the authors consider that the age of (133.37±0.56) –(126.8±0.59) Ma of the Dayin 'gezhuang gold deposit may reflect the activity age of the detachment fault rather than the metallogenic age of the deposit. Given that the metallogenic characteristics of the Dayin 'gezhuang gold deposit are consistent with those of other gold deposits controlled by the Zhaoping, Jiaojia, and Sanshandao fault zones, these gold deposits should have the same metallogenic age. Therefore, the authors of this paper consider that the isotopic age of 118 –119.1 Ma mentioned above reflects the metallogenic age of the Dayin 'gezhuang gold deposit.

5.3. Properties and sources of ore-forming fluids

The ore-forming fluids in the Dayin 'gezhuang gold deposit are generally of H_2O-CO_2-NaCl type with medium-low temperature and medium-low salinity (Yang LQ et al., 2009; Shen K et al., 2000; Chai P et al., 2019a, 2019b). From the early ore-forming stage (I) to the late ore-forming stage (IV), the fluid inclusion types changed from simple to complex and then simple, and the fluids experienced a gradual evolution from high to medium and then low temperature. The salinity ranges of the main ore-forming stages (II and III) are significantly wider than those of the early and late ore-forming stages (I and IV). The H_2O-CO_2 and H_2O solution inclusions were simultaneously trapped in the same fluid inclusion assemblages at the main ore-forming stages (Fig. 10a, b). However, the two types of inclusions have similar final total homogenization temperatures but different salinity values (H_2O solution inclusions have high salinity and H_2O-CO_2 inclusions have low salinity; Fig. 14), indicating that significant fluid immiscibility occurred at the main ore-forming stages (Ramboz C et al., 1982; Roedder E, 1984),

Table 8. Metallogenic age of the Dayin'gezhuang gold deposit.

Sample	Lithology	Mineral	Method	Age/Ma	References
DYGZ-210-3	Pyritization quartz-K-feldspar agglomerates	K-feldspar	^{40}Ar-^{39}Ar	118±1	Lu J, 2012
Y745380KI	Pyrite-sericite-quartz alteration cataclastic rock	Sericite	^{40}Ar-^{39}Ar	130.52±0.52	Yang LQ et al., 2014a
Y745380KII	Pyrite-sericite-quartz alteration cataclastic rock	Muscovite	^{40}Ar-^{39}Ar	128.67±0.50	
Y725245K	Pyrite-sericite-quartz alteration cataclastic rock	Sericite	^{40}Ar-^{39}Ar	133.37±0.56	
Y61250K	Pyrite-sericite-quartz alteration cataclastic rock	Sericite	^{40}Ar-^{39}Ar	126.80±0.59	
DYG-36	Pyrite-sericite-quartz alteration cataclastic rock	Sericite	^{40}Ar-^{39}Ar	119.1±1.2	Yuan ZZ et al., 2019

resulting in contents of volatile constituents such as CO_2 and H_2S in fluids reduced and the gold-bearing complexes decomposed, which led to gold precipitation and mineralization (Bowers TS and Helgeson HC, 1983; Phillips GN and Evans KA, 2004; Chi GX and Xue CJ, 2011; Chai P et al., 2019a).

Many studies have been conducted on the characteristics of ore-forming fluids in the Jiaodong gold deposits, but the sources of ore-forming fluids in these deposits are still controversial. Many researchers believe that the ore-forming fluids were dominated by magmatic water at the main ore-forming stages and were then mixed with meteoric water in the late ore-forming stage (Deng J et al., 2015; Li L et al., 2015; Wen BJ et al., 2016; Liu JC et al., 2017; Cai YC et al., 2018). Some researchers believe that metamorphic water may be the main source of ore-forming fluids in the Jiaodong gold deposits and may be mixed with magmatic water and meteoric water (Yang LQ et al., 2014b, 2016, 2017). Some researchers denied the influence of meteoric water on gold mineralization in the Jiaodong area and believed that the H-O isotopic characteristics are the result of the influence of secondary inclusions after mineralization (Goldfarb RJ and Groves DI, 2015). A few of the H-O isotope values of quartz and sericites in the ores of the Dayin'gezhuang gold deposit fell in the zones of primary magmatic water, metamorphic water, and mantle water, while most of them fell between the zone of Mesozoic meteoric water in the Jiaodong area and the zone of primary magmatic water, metamorphic water, or primary mantle water. The H-O isotopic values of quartz at stage I fell in and near the zones of primary mantle water and primary magmatic water, while those of sericites at stage II/III fell in the zones of primary magmatic water and metamorphic water. Moreover, the H-O isotopic composition gradually drifted to meteoric water from stage I to stage IV (Fig. 15). Considering that the Jiaodong Group has a metamorphic age of approximately 1.8–1.7 Ga (Faure M et al., 2003), which is far earlier than the metallogenic age, the ore-forming fluids unlikely originated from the metamorphic water of the Jiaodong Group. Moreover, this conclusion is also supported by the fact that no metamorphic event occurred in the Dayin' gezhuang mining area during the metallization. Therefore, the fluids in the early ore-forming stage might be magmatic water or mantle water, and then meteoric water gradually entered the ore-forming fluids in the late ore-forming stage.

According to the aforementioned characteristics of fluid inclusions in the Dayin'gezhuang gold deposit, the authors hold that the ore-forming fluids of this deposit originate from mixed sources. Specifically, the early fluids may come from the magmatic fluid system in the process of crust-mantle interactions, and the late fluids may be mixed with much meteoric water. Large-scale magmatism occurred in the Jiaodong area during the gold mineralization of the Dayin' gezhuang gold deposit, forming the Guojialing and Weideshan granites originating from the mixing crust-mantle source, mantle-derived lamprophyres, and the Liulinzhuang high-magnesium diorites originating from of differentiation of mantle-derived materials (Song MC et al., 2020a, 2020b; Wang B et al., 2021). This result indicates that the gold metallogenic period of the Dayin'gezhuang gold deposit was just a period of strong crust-mantle interactions.

5.4. Sources of ore-forming minerals

There are still different understandings of the sources of ore-forming materials in the Jiaodong gold deposits. Researchers holding the view of crust-derived ore-forming materials believe that the metals originate from the Precambrian metamorphic basement and the Upper Jurassic Linglong granites in the Jiaodong area or originate from the Precambrian accretionary metamorphic complexes that were activated and reconstructed during the Mesozoic (Yang LQ et

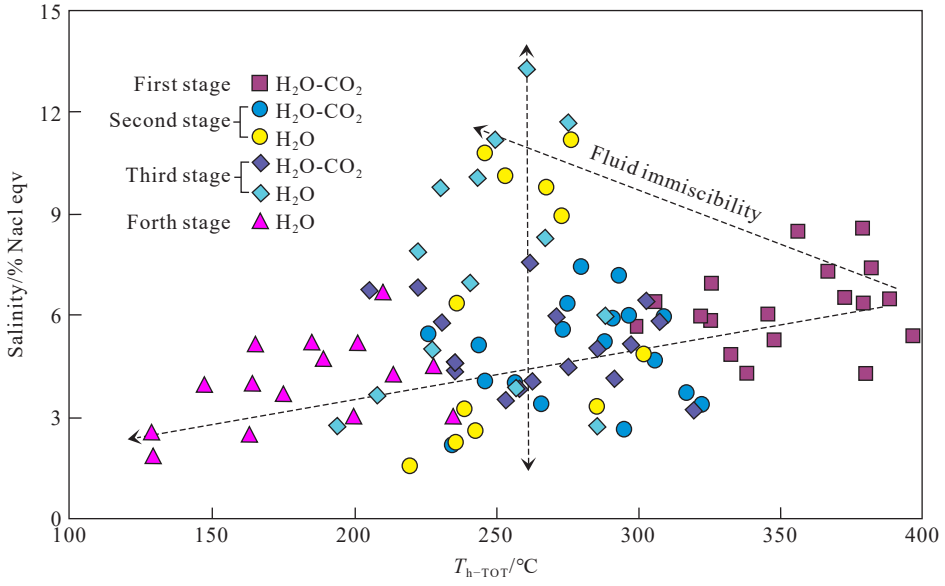

Fig. 14. Plots of total homogenization temperature ($T_{h\text{-}TOT}$) *vs* salinity of fluid inclusions from the Dayin'gezhuang gold deposit. Data source: Chai P et al., 2019a, 2019b; Dai XL, 2012.

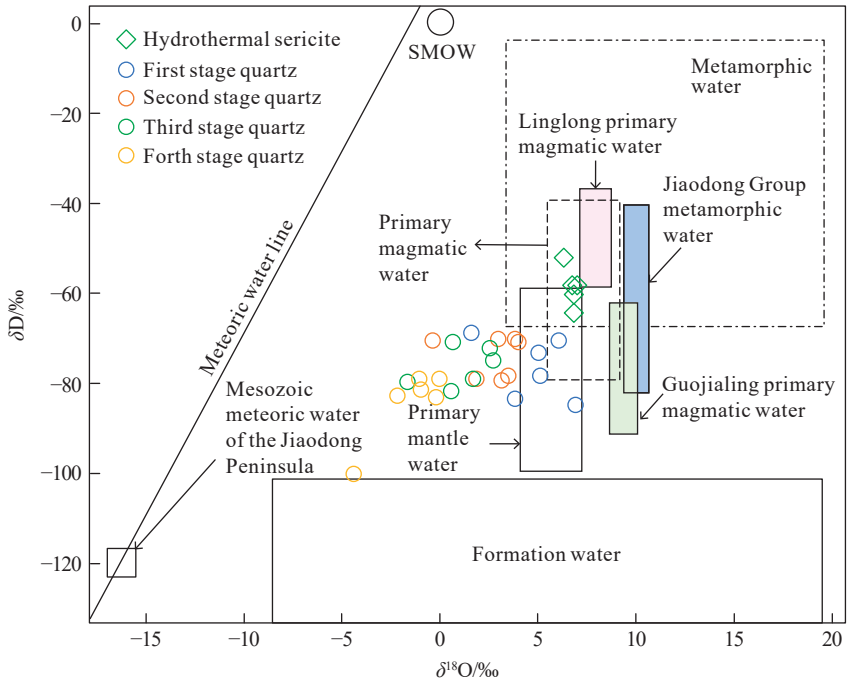

Fig. 15. δD *vs.* δ^{18}O diagram of ore-forming fluids in the Dayin'gezhuang gold deposit (base map from Sheppard SMF, 1996). References are given in Table 5. Fields for Mesozoic meteoric water of the Jiaodong Peninsula, Linglong and Guojialing primary magmatic water, and Jiaodong Group metamorphic water are from Zhang LG et al., 1994, 1995; Mao JW et al., 2005.

al., 2014b). Researchers holding the view of mantle-derived ore-forming materials believe that the metals mainly originate from the deep mantle-derived magmas in the source area of intermediate-mafic dikes (Tan J et al., 2015; Yuan ZZ et al., 2019) and that the enriched mantle-extracted gold to form ores during its partial melting (Wang ZC et al., 2020). Some researchers believe that the enriched lithospheric mantle of the North China Plate has a reservoir with high gold content after undergoing long-term subduction and metasomatism (Deng J et al., 2020a, 2020b). In recent years, some researchers consider that the ore-forming materials are related to the dehydration and desulfurization of the subducted Paleo-Pacific Plate and the devolatilization of the enriched mantle wedge (Deng J et al., 2015; Yang LQ et al., 2016; Liu JC et al., 2018; Wei YJ et al., 2019; Zhang YW et al., 2020).

The S isotopes of the Dayin'gezhuang gold deposit show a positive deviation from meteorite sulfur and a concentrated distribution of $\delta^{34}S_{CDT}$ values, indicating the high homogenization of S. The $\delta^{34}S_{CDT}$ values of the gold deposit largely overlap with those of the Jiaodong Group, the Linglong, Guojialing, and Aishan granites, and intermediate-mafic dikes (Fig. 16), indicating their origins are closely related to each other. The average $\delta^{34}S_{CDT}$ value of the gold deposit is higher than that of the Jiaodong Group and Early Cretaceous mafic dikes containing more mantle components, lower than that of the crust-derived Jingshan Group and close to that of the Linglong granites mainly formed by crustal remelting and that of the Guojialing granites formed by mixed crust-mantle melting (Hou ML et al., 2007; Wang ZL et al., 2014). These results indicate that the S source has the characteristics of crust-mantle interactions.

As shown in the $^{207}Pb/^{204}Pb$ *vs.* $^{206}Pb/^{204}Pb$ diagram (Fig. 17), all the Pb isotope values of the Dayin'gezhuang gold deposit fell between the mantle and orogen evolution lines and show a linear distribution trend, except one value, which fell on the upper crust evolution line. Moreover, the Pb isotope values of the Jiaodong Group fell between the mantle and upper crust evolution lines or near the mantle and lower crust evolution lines. The Pb isotope values of the Linglong granites fell near the mantle evolution line and between the mantle and lower crust evolution lines. The Pb isotope values of the Guojialing granites generally fell between or near the mantle and orogen evolution lines. All these results indicate the characteristics of mixed crust- and mantle-derived Pb. The Pb isotope values of the ores in the Dayin 'gezhuang gold deposit largely overlapped with those of the main geological bodies in the Jiaodong area, indicating that ores share the material sources with and inheriting properties from their surrounding rocks (i.e., the Linglong granites and the Jiaodong Group).

The S and Pb isotopic characteristics of the Dayin 'gezhuang gold deposit are similar to those of the ore-hosting rocks, and the $\delta^{34}S_{CDT}$ values of the deposit are distributed more intensively than those of the ore-hosting rocks. This result indicates that the metallogenic materials mainly originate from ore-hosting rocks. Since the Jiaodong area underwent strong crust-mantle interactions during the Early Cretaceous, the ore-hosting rocks are dominated by crust-derived materials and are significantly mixed with mantle-derived materials. Therefore, the authors of this paper hold that the Dayin 'gezhuang gold deposit mainly has crust-derived ore-forming materials, which also contain a small quantity of mantle-derived materials.

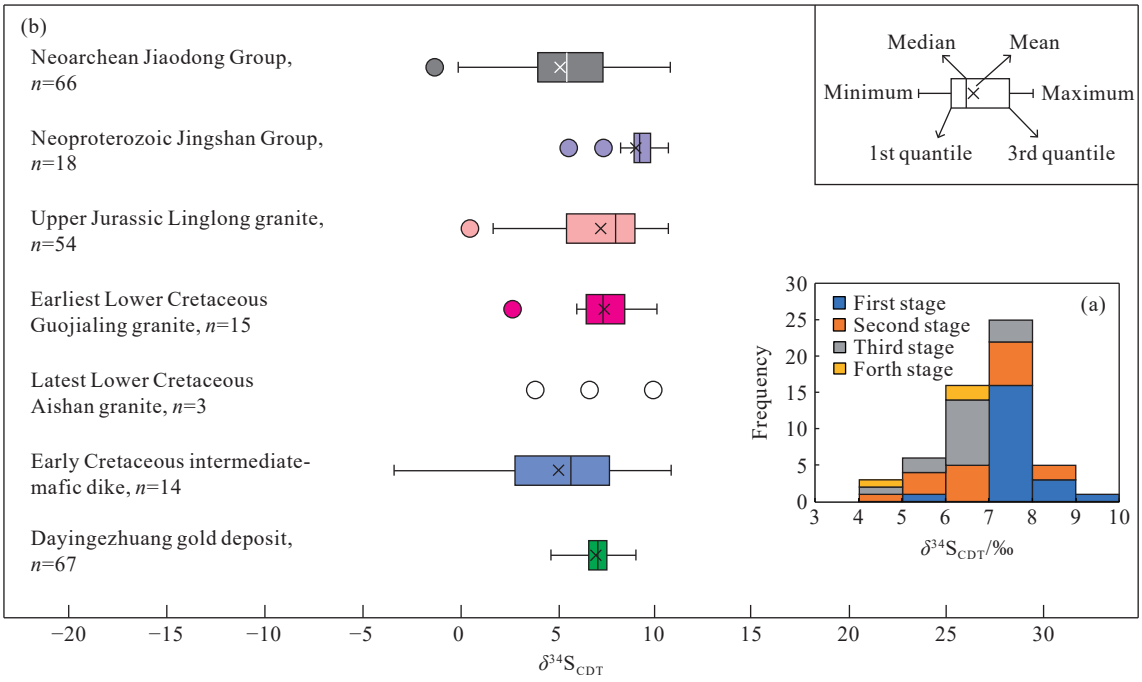

Fig. 16. a–Sulfur isotopic histogram in the Dayin'gezhuang gold deposit; b–comparison of sulfur isotopic compositions between Dayin'gezhuang gold deposit, Jiaodong Group, Jingshan Group, Mesozoic magmatic rocks, and intermediate-mafic dikes. Data source: Li ZL and Yang MZ, 1993; Mao JW et al., 2005; Hou ML et al., 2006; Dai XL, 2012; Zhang RZ et al., 2016; Yuan ZZ et al., 2019.

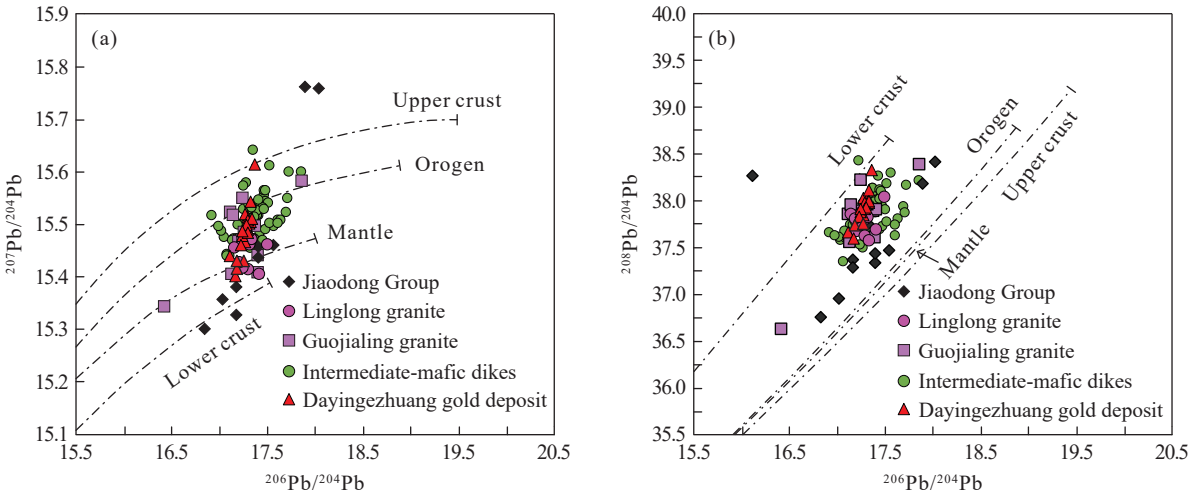

Fig. 17. Lead isotopic compositions of the Dayin'gezhuang gold deposit, shown on $^{207}Pb/^{204}Pb$ *vs.* $^{206}Pb/^{204}Pb$ (a) and $^{208}Pb/^{204}Pb$ *vs.* $^{206}Pb/^{204}Pb$ (b). Data source: Cai YC et al., 2013; Chen ZS et al., 1994; Guan K et al., 1997; Li ZL and Yang MZ, 1993; Liu XF et al., 2018; Ma L et al., 2014; Ma ZD, 1998; Mao JW et al., 2005; Tan J et al., 2012; Yang SW et al., 1986; Yuan ZZ et al., 2019.

5.5. Genesis and metallogenic process of the Dayin'gezhuang gold deposit

The Dayin'gezhuang gold deposit is hosted in the Zhaoping Fault zone. The hanging wall of this fault zone is mainly composed of Precambrian metamorphic rocks, and the footwall of the fault is composed of Upper Jurassic Linglong granites. Many mafic dikes are distributed in the deposit, and there are still Earliest Lower Cretaceous Guojialing and Weideshan granites (such as Aishan and Nansu plutons) near the deposit. These geological bodies and fault structures are closely related to gold mineralization. According to the diagenetic and metallogenic time, the geological bodies related to the Jiaodong gold deposits can be divided into ore-hosting geological bodies (including Precambrian metamorphic rocks and Linglong and Guojialing granites) and geological bodies during the ore-forming period (including Weideshan granites and mafic dikes). As indicated by relevant studies, the Linglong and Guojialing granites have the characteristics of adakites and resulted from the partial melting of the paleocrust (Wang B et al., 2021); the Weideshan granites have the characteristics of arc granites and arose from the partial melting of the juvenile lower crust, and the occurrence of dioritic inclusions in Weideshan granites and the widespread distribution of mafic dikes in the deposit indicate the existence of mantle-derived magmatism

(Song MC et al., 2020b). These results indicate that gold mineralization occurred during the transition from adakitic granites to arc granites and the crust-mantle interactions. As shown by the thermochronological study results of granites, the Linglong granites slowly cooled from approximately 800°C at their formation age of 160 Ma to approximately 450±50°C at approximately 143 Ma (Charles N et al., 2013); the Guojialing granites cooled at a rate of 100°C/Ma from 130–126 Ma to 124 Ma; the Weideshan granites experienced a more rapid cooling process after forming and rapidly cooled to approximately 350±50°C at 122 –118 Ma, and granites cooled at a rate of above 30°C/Ma at 117–110 Ma (Wu L et al., 2018). The thermochronological study of Jiaodong gold deposits after mineralization shows that they have experienced a very slow cooling and uplifting process since approximately 95 Ma, with a cooling rate of 0.4 –2.4°C/Ma (Zhang QB et al., 2022). Therefore, the gold mineralization was accompanied by rapid crustal uplifting and cooling.

Based on the geological process characteristics related to gold mineralization mentioned above, the authors hold that the formation of the Dayin'gezhuang gold deposit is related to crust-mantle interactions, granite emplacement, the transformation of geochemical properties, and rapid crustal uplifting and that the Dayin 'gezhuang gold deposit was formed by thermal-uplift and extensional tectonism (Song MC et al., 2014, 2022a). During the Upper Jurassic, the large-scale continental crust in the Jiaodong area remelted due to the post-collision and compression of the North China Plate and Yangtze Block, as well as the crustal thickening caused by the subduction of the Paleo-Pacific Plate or the Izanagi plate toward the Asian Continent, forming Linglong granites (Zhang YQ et al., 2007). During the Lower Cretaceous, the paleo North China Plate was destroyed due to the subduction and retreat of the Paleo-Pacific Plate. As a result, the lithosphere and the crust intensively thinned, and the asthenosphere upwelled, leading to intense crust-mantle material exchange (Zhu RX et al., 2011). The partial melting of the enriched lithospheric mantle produced mafic magmas, and the underplating of mantle-derived mafic magmas acted on the paleo or juvenile crust at the bottom, causing the partial melting of the rocks at the crust bottom (Qiu LG et al., 2008). Mantle-derived mafic magmas intruded upward and differentiated, forming lamprophyres and other dark dikes. Moreover, different degrees of mixing, crystallization, and differentiation of mantle- and crust-derived magmas formed Guojialing, Weideshan, and Laoshan granites (Wang B et al., 2021). The strong crust-mantle interactions, large-scale magmatism, and the material exchange arising from the transformation from adakitic granites to arc granites and from the ancient lower crust to the juvenile lower crust indicated by the granite transformation during the Lower Cretaceous provided abundant fluids and material sources for gold mineralization. The large-scale magmatism during the Lower Cretaceous was accompanied by the rapid uplifting of intrusions and the crust and strong extensional tectonism, forming a thermal-uplift extensional tectonic system (Song MC et al, 2015, 2018). Since the rapid uplift of magmas strongly jacked up the shallow surrounding rocks, many extensional fracture structures were formed in the early Linglong granites, and detachment faults were formed along the interface between the Linglong granites and the Precambrian metamorphic rocks, creating favorable space for accumulation and mineralization of ore-forming fluids. Moreover, as the magmas were uplifted rapidly, the temperature and pressure of fluids dropped sharply, resulting in immiscibility (phase separation) or boiling. Consequently, large numbers of components such as CO_2, and H_2S escaped, the pH of the system increased, and fluids containing metal elements such as Fe and Cu reacted with the fluids containing S, forming sulfides such as pyrites and chalcopyrite. The escape and consumption of components such as CO_2 and H_2S reduced the stability of gold-bearing complex compounds in the fluids. Finally, golds in the form of native gold and electrum were precipitated and mineralized along with metal sulfides such as pyrites at the pressure fluctuation parts, i.e., the high-to-low transition parts of the dip angle of detachment faults (Fig. 18).

6. Conclusions

(i) The Dayin'gezhuang gold deposit is a supergiant gold deposit with total resources of more than 180 t and consists of No. 1 and No. 2 orebodies. The orebodies in the deposit are distributed with the regularity of pinch-out and recurrence, and ore-free intervals exist between the deep and shallow orebodies. The orebodies have a pitch direction of NNE, a pitch angle of approximately 55°, a plunge direction of NEE 75°, and a plunge angle of approximately 22°. The ore-controlling Zhaoping Fault is a shovel-shaped stepped fault, and the fault dip angle presents three sections of stepped high-to-low transitions at an elevation of −2000 –0 m. The gold mineralization enrichment areas are mainly distributed in the high-to-low transition parts of the dip angle and the relatively gentle steps, forming a stepped pattern from shallow to deep.

(ii) The Dayin 'gezhuang gold deposit was formed at approximately 120 Ma. The ore-forming fluids were H_2O-CO_2-NaCl-type hydrothermal solutions with medium-low temperature and medium-low salinity. The fluids evolved from high to medium and then low temperature, and the fluid immiscibility occurred at the main ore-forming stages (II and III). The H-O isotopic characteristics indicate that the early fluids may originate from the magmatic fluid system with crust-mantle interactions, and the late fluids may have been mixed with much meteoric water. The S and Pb isotopic characteristics indicate that the Dayin'gezhuang gold deposit mainly has crust-derived ore-forming materials, which also contain a small quantity of mantle-derived materials.

(iii) The Dayin 'gezhuang gold deposit was formed by thermal uplift and extensional tectonism. The strong crust-mantle interactions, large-scale magmatism, and the material exchange arising from the transformation from adakitic granites to arc granites and from the ancient lower crust to the juvenile lower crust during the Lower Cretaceous provided

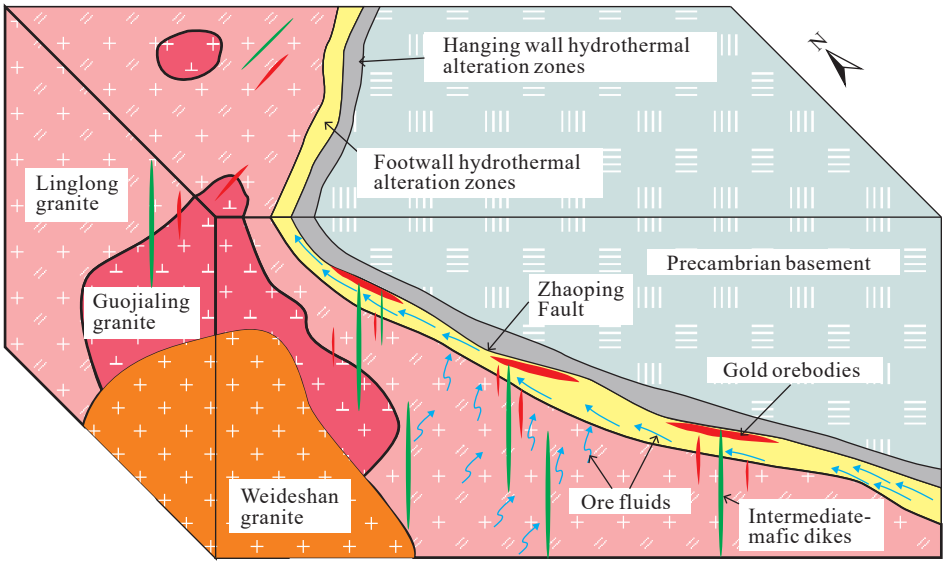

Fig. 18. A proposed cartoon illustrating the ore genesis of the Dayin'gezhuang gold deposit.

abundant fluids and material sources for mineralization. Moreover, the detachment faults formed by the rapid magmatic uplift and the extensional tectonism created favorable temperature and pressure conditions and space for fluid accumulation and gold precipitation and mineralization.

CRediT authorship contribution statement

Ming-chun Song, Zheng-jiang Ding and Ming-ling Zhou conceived and designed the ideas. Xiang-dong Liu prepared the manuscript, and drew all the figures. Shao-hui Xu, Zhen-liang Yang, Tian-ci Xie, Xue-kan Gao, Rui-xiang Li participated in field investigation. Liang-liang Zhang, Qi-bin Zhang, Shan-shan Wang, and Bin Wang performed the data processing. Tao Cui and Ying-xin Song reviewed and edited the draft. All authors discussed the results and contributed to the final manuscript.

Declaration of competing interest

The authors declare no conflicts of interest.

Acknowledgment

Professor Kun-feng Qiu and Researcher Jun-jian Li reviewed the entire manuscript and proposed valuable comments. The authors hereby would like to extend their sincere gratitude to them. This paper was financially supported by the NSFC-Shandong Joint Fund Program entitled "Control Mechanisms of Faults on Deep Gold Deposits in Jiaodong Peninsula" (Grant No. U2006201), Science and Technology Project of Shandong Bureau of Geology and Mineral Exploration and Development entitled "Fault system and its relationship with gold mineralization, northwestern Jiaodong Peninsula" (Grant No. KY202208) and Open Fund of Big Data Application and Development Engineering Laboratory for Deep Gold Exploration in Shandong Province entitled "Ore-forming fluid and ore-forming material source of Jiudian gold deposit, Jiaodong" (Grant No. SDK202211).

References

Ames L, Zhou GZ, Xiong BC. 1996. Geochronology and isotopic character of ultrahigh-pressure metamorphism with implications for collision of the Sino-Korean and Yangtze cratons, central China. Tectonics, 15(2), 472–489. doi: 10.1029/95TC02552.

Bowers TS, Helgeson HC. 1983. Calculation of thermodynamic and geochemical consequences of nonideal mixing in the system H_2O-NaCl-CO_2 on phase relations in geologic system: Equation of state for H_2O-NaCl-CO_2 fluids at high pressure and temperatures. Geochimica et Cosmochimica Acta, 47(7), 1247–1275. doi: 10.1016/0016-7037(83)90066-2.

Cai YC, Fan HR, Santosh M, Liu X, Hu FF, Yang KF, Lan TG, Yang YH, Liu YS. 2013. Evolution of the lithospheric mantle beneath the southeastern North China Craton: Constraints from mafic dikes in the Jiaobei terrain. Gondwana Research, 24, 601–621. doi: 10.1016/j.gr.2012.11.013.

Cai YC, Fan HR, Santosh M, Hu FF, Yang KF. 2018. Decratonic gold mineralization: Evidence from the Shangzhuang gold deposit, eastern North China Craton. Gondwana Research, 54, 1–22. doi: 10.1016/j.gr.2017.09.009.

Chai P, Zhang ZY, Hou ZQ. 2019a. Geological and fluid inclusion constraints on gold deposition processes of the Dayingezhuang gold deposit, Jiaodong Peninsula, China. Acta Geologica Sinica (English Edition), 93(4), 955–971. doi: 10.1111/1755-6724.13849.

Chai P, Zhang HR, Dong LL. Zhang ZY. 2019b. Geology and ore-forming fluids of the Dayingezhuang gold deposit, Jiaodong Peninsula, eastern China: Implications for mineral exploration. Journal of Geochemical Exploration, 204, 224–239. doi: 10.1016/j.gexplo.2019.06.001.

Charles N, Augier R, Gumiaux C, Monié P, Chen Y, Faure M, Zhu RX. 2013. Timing, duration and role of magmatism in wide rift systems: Insights from the Jiaodong Peninsula (China, East Asia). Gondwana Research, 24(1), 412–428. doi: 10.1016/j.gr.2012.10.011.

Chen J, Mao XC, Deng H. 2020a. 3D Quantitative mineral prediction in the depth of the Dayingezhuang gold deposit, Shandong Province. Acta Geoscientica Sinica, 41(2), 179–191 (in Chinese with English abstract). doi: 10.3975/cagsb.2020.020701.

Chen J, Mao XC, Liu ZK, Deng H. 2020b. Three-dimensional

metallogenic prediction based on random forest classification algorithm for the Dayingezhuang gold deposit. Geotectonica et Metallogenia, 44(2), 231–241 (in Chinese with English abstract).

Chen JF, Xie Z, Li HM. 2003. U-Pb zircon ages for a collision-related K-rich complex at Shidao in the Sulu ultrahigh pressure terrane, China. Geochemical Journal, 37, 35–46. doi: 10.2343/geochemj.37.35.

Chen JZ, Jiang N. 2011. Petrogenesis of the Late-Triassic alkaline magmatism in the Jiaodong area: Evidence from U-Pb age, Hf-O isotopes of zircons. Acta Petrologica Sinica, 27(12), 3557–3574 (in Chinese with English abstract).

Chen ZS, Zhang LG, Liu JX, Wang BC, Xu JF, Zheng WS. 1994. A study on lead isotope geochemical backgrounds of geological bodies in Jiaodong region. Contributions to Geology and Mineral Resources Research, 9(1), 65–78 (in Chinese with English abstract). doi: 10.6053/j.issn.1001-1412.1994.1.008.

Chi GX, Xue CJ. 2011. Abundance of CO_2-rich fluid inclusions in a sedimentary basin hosted Cu deposit at Jinman, Yunnan: Implications for mineralization environment and classification of the deposit. Mineralium Deposita, 46(4), 365–380. doi: 10.1007/s00126-011-0337-8.

Chough SK, Sohn YK. 2010. Tectonic and sedimentary evolution of a Cretaceous continental arc-backarc system in the Korean peninsula: New view. Earth Science Review, 101(3–4), 225–249. doi: 10.1016/j.earscirev.2010.05.004.

Clayton RN, O'Neil JR, Mayeda TK. 1972. Oxygen isotope exchange between quartz and water. Journal of Geophysical Research, 77(17), 3057–3067. doi: 10.1029/JB077i017p03057.

Dai XL. 2012. Study on Petrogenesic-Mentallogenic Mechanism in Dayingezhuang Gold Deposit, Zhaoyuan Country, Shandong Province. Changsha, Zhongnan University, Ph. D. thesis, 1–151 (in Chinese).

Deng H, Zheng Y, Chen J, Wei YF, Mao XC. 2020. Deep learning-based 3d prediction model for the Dayingezhuang gold deposit, Shandong Province. Acta Geoscientica Sinica, 41(2), 157–165 (in Chinese with English abstract). doi: 10.3975/cagsb.2020.020501.

Deng J, Wang QF, Wan L, Liu H, Yang LQ, Zhang J. 2011. A multifractal analysis of mineralization characteristics of the Dayingezhuang disseminated-veinlet gold deposit in the Jiaodong gold province of China. Ore Geology Reviews, 40(1), 54–64. doi: 10.1016/j.oregeorev.2011.05.001.

Deng J, Liu XF, Wang QF, Pan RG. 2015. Origin of the Jiaodong-type Xinli gold deposit, Jiaodong Peninsula, China: Constraints from fluid inclusion and C-D-O-S-Sr isotope compositions. Ore Geology Reviews, 65, 674–686. doi: 10.1016/j.oregeorev.2014.04.018.

Deng J, Wang QF. 2016. Gold mineralization in China: Metallogenic provinces, deposit types and tectonic framework. Gondwana Research, 36, 219–274. doi: 10.1016/j.gr.2015.10.003.

Deng J, Liu XF, Wang QF, Dilek Y, Liang YY. 2017. Isotopic characterization and petrogenetic modeling of Early Cretaceous mafic diking-Lithospheric extension in the North China craton, eastern Asia. GSA Bulletin, 129(11–12), 1379–1407. doi: 10.1130/B31609.1.

Deng J, Yang LQ, Li RH, Groves DI, Santosh M, Wang ZL, Sai SX, Wang SR. 2019. Regional structural control on the distribution of world-class gold deposits: An overview from the Giant Jiaodong Gold Province, China. Geological Journal, 54(1), 378–391. doi: 10.1002/gj.3186.

Deng J, Yang LQ, Groves DI, Zhang L, Wang QF. 2020a. An integrated mineral system model for the gold deposits of the giant Jiaodong province, eastern China. Earth-Science Reviews, 208(2), 103274. doi: 10.1016/j.earscirev.2020.103274.

Deng J, Wang QF, Santosh M, Liu XF, Liang YY, Yang LQ, Zhao R, Yang L. 2020b. Remobilization of metasomatized mantle lithosphere: A new model for the Jiaodong gold province, eastern China. Mineralium Deposita, 55(2), 257–274. doi: 10.1007/s00126-019-00925-0.

Deng J, Qiu KF, Wang QF, Goldfarb R, Yang LQ, Zi JW, Geng JZ, Ma Y. 2020C. In situ dating of hydrothermal monazite and implications for the geodynamic controls on ore formation in the Jiaodong Gold Province, Eastern China. Economic Geology, 115(3), 671–685. doi: 10.5382/econgeo.4711.

Fan HR, Lan TG, Li XH, Santosh M, Yang KF, Hu FF, Feng K, Hu HL, Peng HW, Zhang YW. 2021. Conditions and processes leading to large-scale gold deposition in the Jiaodong province, eastern China. Science China Earth Sciences, 64(9), 1504–1523 (in Chinese with English abstract). doi: 10.1007/s11430-020-9789-2.

Faure M, Lin W, Monie P, Breton NL, Poussineau S, Panis D, Deloule E. 2003. Exhumation tectonics of the ultrahigh-pressure metamorphic rocks in the Qinling orogen in East China: New petrological-structural-radiometric insights from the Shandong Peninsula. Tectonics, 22(3), 1018–1040. doi: 10.1029/2002TC001450.

Gao TS, Chen JF, Xie Z, Yan J, Qian H. 2004. Geochemistry of Triassic igneous complex at Shidao in the Sulu UHP metamorphic belt. Acta Petrologica Sinica, 20(5), 1025–1038 (in Chinese with English abstract). doi: 10.3969/j.issn.1000-0569.2004.05.004.

Geng K, Wang RJ, Li HK, Liang TT, Zhang YB. 2016. Zircon SHRIMP U-Pb geochronology of Congjia granodiorite from Northwest Jiaodong Area. Acta Geoscientica Sinica, 37(1), 90–100 (in Chinese with English abstract). doi: 10.3975/cagsb.2016.01.09.

Goldfarb RJ, Groves DI. 2015. Orogenic gold: Common or evolving fluid and metal sources through time. Lithos, 233, 2–26. doi: 10.1016/j.lithos.2015.07.011.

Goss SC, Wilde SA, Wu FY, Yang JH. 2010. The age, isotopic signature and significance of the youngest Mesozoic granitoids in the Jiaodong Terrane, Shandong Province, North China Craton. Lithos, 120(3–4), 309–326. doi: 10.1016/j.lithos.2010.08.019.

Guan K, Luo ZK, Miao LC, Huang JZ. 1997. Petrochemical and geochemical characteristics of Guojialing suite granite in Zhaoye district and the genetic relation of gold mineralization to the granite. Contributions to Geology and Mineral Resources Research, 12(4), 1–8 (in Chinese with English abstract).

Guo JH, Chen FK, Zhang XM, Siebel W, Zhai MG. 2005. Evolution of syn- to post-collisional magmatism from north Sulu UHP belt, eastern China: Zircon U-Pb geochronology. Acta Petrologica Sinica, 21(4), 1281–1301 (in Chinese with English abstract). doi: 10.3969/j.issn.1000-0569.2005.04.025.

Hagemann SG, Lüders V. 2003. P-T-X conditions of hydrothermal fluids and precipitation mechanism of stibnite-gold mineralization at the Wiluna lode-gold deposits, Western Australia: Conventional and infrared microthermometric constraints. Mineralium Deposita, 38(8), 936–952. doi: 10.1007/s00126-003-0351-6.

Hou ML, Jiang SY, Jiang YH, Ling HF. 2006. S-Pb isotope geochemistry and Rb-Sr geochronology of the Penglai gold field in the eastern Shandong province. Acta Petrologica Sinica, 22(10), 2525–2533 (in Chinese with English abstract). doi: 10.3969/j.issn.1000-0569.2006.10.013.

Hou ML, Jiang YH, Jiang SY, Ling HF, Zhao KD. 2007. Contrasting origins of Late Mesozoic adakitic granitoids from the northwestern Jiaodong Peninsula, East China: Implications for crustal thickening to delamination. Geological Magazine, 144(4), 619–631. doi: 10.1017/S0016756807003494.

Jiang N, Chen JZ, Guo JH, Chang GH. 2012. In situ zircon U-Pb, oxygen and hafnium isotopic compositions of Jurassic granites from the North China Craton: Evidence for Triassic subduction of continental crust and subsequent metamorphism-related ^{18}O depletion. Lithos, 142–143, 84–94. doi: 10.1016/j.lithos.2012.02.018.

Li DX, Gao BF, Liu Y, Zhou YH, Jiang SQ, Xu FY, Zhu YR, Yu RY, Xu JL, Wang CH, Zhang RZ, Wu Z. 2006. Structural controls and

ore prospecting in the Dayingezhuang gold deposit. Geology and Prospecting, 42(4), 32–35 (in Chinese with English abstract). doi: 10.3969/j.issn.0495-5331.2006.04.007.

Li H, Zheng T, Tang L, Xu Z, Wang XJ, Li JX. 1998. Super imposed halo model used for positional predication of the concealed ore bodies in the Dayingezhuang gold deposit, Zhaoyuan, Shandong. Geological Exploration for Non-ferrous Metals, 7(3), 178–181 (in Chinese with English abstract).

Li JL, Zhang YQ, Liu ZQ, Ren FL, Yuan JY. 2007. Sedimentary-subsidence history and tectonic evolution of the Jiaolai basin, eastern China. Geology in China, 34(2), 240–250 (in Chinese with English abstract). doi: 10.3969/j.issn.1000-3657.2007.02.005.

Li L, Santosh M, Li SR. 2015. The "Jiaodong type" gold deposits: Characteristics, origin and prospecting. Ore Geology Reviews, 65, 589–611. doi: 10.1016/j.oregeorev.2014.06.021.

Li SJ. 1998. Division and correlation of Jurassic and Cretaceous strata in Shandong. Journal of the University of Petroleum, China, 22(1), 1–4 (in Chinese with English abstract).

Li SY, Li J, Song MC, Ding ZJ, Zhou ML, Fan JM, Xie TC, Liu XD, Wang B, Zhang LL, Yang ZL. 2022. Metallogenic characteristics and mineralization of the Linglong gold field, Jiaodong Peninsula. Acta Geologica Sinica, 96(9), 1–28 (in Chinese with English abstract). doi: 10.19762/j.cnki.dizhixuebao.2022291.

Li ZL, Yang MZ. 1993. The Geology-Geochemistry of Gold Deposits in Jiaodong Region. Tianjin, Tianjin Science and Tecnology Press, 10–64 (in Chinese).

Lin WW, Zhao YM, Xu J. 2000. Active properties and age of Zhaoyuan-Pingdu fracture zone. Regional Geology of China, 19(1), 43–50 (in Chinese with English abstract). doi: 10.3969/j.issn.1671-2552.2000.01.008.

Liu JC, Wang JY, Liu Y, Tian JX, Li XZ, Zhang HD. 2017. Ore genesis of the Xiadian gold deposit, Jiaodong Peninsula, East China: Information from fluid inclusions and mineralization. Geological Journal, 53(51), 77–95. doi: 10.1002/gj.3042.

Liu LS, Liu FL, Ji L, Wang W, Wang F, Cai J, Liu PH. 2018. The polygenetic meta-granitic rocks and their geological significance, within the North Sulu ultrahigh-pressure belt. Acta Petrologica Sinica, 34(6), 1557–1580 (in Chinese with English abstract).

Liu XD. 2022. Deep Prospecting Prediction of Typical Gold Deposits in the Zhaoping Gold Belt, Jiaodong Peninsula, China. Beijing, China University of Geoscience (Beijing), Ph. D. thesis, 1–149 (in Chinese with English abstract).

Liu XF, Deng J, Yang LQ, Wang QF, Pan RG, Qin C, Yang Y. 2018. Petrogenesis of Early Cretaceous intermediate-felsic dikes in the Jiaodong Peninsula, south-eastern North China Craton: Constraints from geochronology, geochemistry and Sr-Nd-Pb-Hf isotopes. Gondwana Research, 60, 69–93. doi: 10.1016/j.gr.2018.04.005.

Liu Y, Deng J, Wang ZL, Zhang L, Zhang C, Liu XD, Zheng XL, Wang XD. 2014. Zircon U-Pb age, Lu-Hf isotopes and petrogeochemistry of the monzogranites from Xincheng gold deposit, northwestern Jiaodong Peninsula, China. Acta Petrologica Sinica, 30(9), 2559–2573 (in Chinese with English abstract).

Liu Y, Yang LQ, Guo LN, Li RH, Gao BF, Meng YS, Zhang RZ. 2014. Composition of ore-forming fluids in the Dayingezhuang gold deposit of the Jiaodong Peninsula, China. Acta Petrologica Sinica, 30(9), 2507–2517 (in Chinese with English abstract).

Lu J. 2012. The Ore-Forming Fluid Characteristics and Mineralogenetic Epoch of the Dayingezhuang Gold Deposit in Jiaodong region. Beijing, China University of Geoscience (Beijing), Master thesis, 1–82(in Chinese).

Ma L, Jiang SY, Dai BZ, Jiang YH, Hou ML, Pu W, Xu B. 2013. Multiple sources for the origin of Late Jurassic Linglong adakitic granite in the Shandong Peninsula, eastern China: Zircon U-Pb geochronological, geochemical and Sr-Nd-Hf isotopic evidence. Lithos, 162–163, 251–263. doi: 10.1016/j.lithos.2013.01.009.

Ma L, Jiang SY, Hou ML, Dai BZ, Jiang YH, Yang T, Zhao KD, Pu W, Zhu ZY, Xu B. 2014. Geochemistry of Early Cretaceous calc-alkaline lamprophyres in the Jiaodong Peninsula: Implication for lithospheric evolution of the eastern North China Craton. Gondwana Research, 25, 859–872. doi: 10.1016/j.gr.2013.05.012.

Ma XH, Zeng QW, Tao SY, Cao R, Zhou ZH. 2021. Mineralogical characteristics and in-situ sulfur isotopic analysis of gold-bearing sulfides from the Qilishan gold deposit in the Jiaodong Peninsula, China. Journal of Earth Science, 32(1), 116–126. https://doi.org/10.1007/s12583-020-1370-2.

Ma YX, Hu JH, Chang YJ, Liu ZJ. 2021. Study on the coincident-loop transient electromagnetic method in seafloor exploration —Taking Jiaodong Polymetallic mine as a model. Journal of Earth Science, 32(1), 25–41. https://doi.org/10.1007/s12583-020-1087-2.

Ma ZD. 1998. Discussion on characteristic of lead isotope composition of original gold deposits in Sino-Korean Paralatfrom and relation to some problems. Earth Science, 13(4), 395–402 (in Chinese with English abstract).

Mao JW, Hua RM, Li XB. 1999. A preliminary study of large-scale metallogenesis and large clusters of mineral deposits. Mineral Deposits, 18(4), 291–299 (in Chinese with English abstract). doi: 10.3969/j.issn.0258-7106.1999.04.001.

Mao JW, Li HM, Wang YT, Zhang CQ, Wang RT. 2005. The relationship between mantle-derived fluid and gold ore-formation in the eastern Shandong Peninsula: Evidences from D-O-C-S isotopes. Acta Geologica Sinica, 79(6), 839–857 (in Chinese with English abstract). doi: 10.3321/j.issn:0001-5717.2005.06.013.

Mao XC, Ren J, Liu ZK, Chen J, Tang L, Deng H, Bayless RC, Yang B, Wang MJ, Liu CM. 2019. Three-dimensional prospectivity modeling of the Jiaojia-type gold deposit, Jiaodong Peninsula, Eastern China: A case study of the Dayingezhuang deposit. Journal of Geochemical Exploration, 203, 27–44. doi: 10.1016/j.gexplo.2019.04.002.

Mao XC, Wang MJ, Liu ZK, Chen J, Deng H. 2019. Quantitative analysis of ore-controlling factors based on exploration data of the Dayingezhuang gold deposit in the Jiaodong Peninsula. Earth Science Frontiers, 26(4), 84–93 (in Chinese with English abstract). doi: 10.13745/j.esf.2019.04.010.

Phillips GN, Evans KA. 2004. Role of CO_2 in the formation of gold deposits. Nature, 429(6994), 860–863. doi: 10.1038/nature02644.

Qiu LG, Ren FL, Cao ZX, Zhang YQ. Late mesozoic magmatic activities and their constraints on geotectonics of Jiaodong region. Geotectonica et Metallogenia, 32(1), 117 –123 (in Chinese with English abstract). doi: 10.3969/j.issn.1001-1552.2008.01.015.

Ramboz C, Pichavant M, Weisbrod A. 1982. Fluid immiscibility in natural processes: Use and misuse of fluid inclusion data: II. Interpretation of fluid inclusion data in terms of immiscibility. Chemical Geology, 37(1 –2), 29 –48. doi: 10.1016/0009-2541(82)90065-1.

Ren FL, Liu ZQ, Qiu LG, Han LG, Zhang YQ, Cao ZX. 2008. The prototype character of Jiaolai Basin in Cretaceous Laiyang Period. Acta Sedimentologica Sinica, 26(2), 221–232 (in Chinese with English abstract). doi: 10.14027/j.cnki.cjxb.2008.02.006.

Roedder E. 1984. Fluid inclusions. Review Mineralogy, 12, 1–664. doi: 10.2465/minerj.12.1.

Shen K, Hu SX, Sun JG, Ling HF, Zhao YY, Sun MZ. 2000. Characteristics of ore-forming fluids of the Dayingezhuang gold deposit in Eastern Shandong, China. Acta Petrologica Sinica, 16(4), 542–550 (in Chinese with English abstract). doi: 10.3969/j.issn.1000-0569.2000.04.013.

Shen YK, Guo T, Lü ZC, Deng J, Yang YQ, Zhao ZJ, Wang CL. 2022. Analysis on the ore-controlling structures and prospecting in the Dayingezhuang gold deposit, Zhaoyuan, Shandong. Geology in China, 49(1), 215–225 (in Chinese with English abstract). doi: 10.12029/gc20220113.

Sheppard SMF. 1996. Characterization and isotopic variations in natural waters. Reviews in Mineralogy, 16(1), 165–183. doi: 10.1109/PDMCHiBi.2010.11.

Song MC, Yi PH, Xu JX, Cui SX, Shen K, Jiang HL, Yuan WH, Wang HJ. 2012. A step metallogenetic model for gold deposits in the northwestern Shandong Peninsula, China. Science China Earth Science, 55(6), 940–948. doi: 10.1007/s11430-012-4366-7.

Song MC, Li SZ, Yi PH, Cui SX, Xu JX, Lü GX, Song YX, Jiang HL, Zhou ML, Zhang PJ, Huang TL, Liu CC, Liu DH. 2014. Classification and metallogenic theory of the Jiaojia-style gold deposit in Jiaodong Peninsula, China. Journal of Jilin University (Earth Science Edition), (1), 87–104. doi: 10.13278/j.cnki.jjuese.201401108.

Song MC, Li SZ, Santosh M, Zhao SJ, Yu S, Yi PH, Cui SX, Lü GX, Xu JX, Song YX Zhou ML. 2015. Types, characteristics and metallogenesis of gold deposits in the Jiaodong Peninsula, Eastern North China Craton. Ore Geology Reviews, 65, 612–625. doi: 10.1016/j.oregeorev.2014.06.019.

Song MC, Li J, Li SY, Ding ZJ, Tan XF, Zhang ZL, Wang SJ. 2018. Late Mesozoic thermal upwelling-extension structure and its dynamics back-ground in eastern Shandong Province. Journal of Jilin University (EarthScienceEdition), 48(4), 941–964. doi: 10.13278/j.cnki.jjuese.20170145.

Song MC, Lin SY, Yang LQ, Song YX, Ding ZJ, Li J, Li SY, Zhou ML. 2020a. Metallogenic model of Jiaodong Peninsula gold deposits. Mineral Deposits, 39, 215–236 (in Chinese with English abstract). doi: 10.16111/j.0258-7106.2020.02.002.

Song MC, Zhou JB, Song YX, Wang B, Li SY, Li J, Wang SS. 2020b. Mesozoic Weideshan granitoid suite and its relationship to large-scale gold mineralization in the Jiaodong Peninsula, China. Geological Journal, 55, 5703–5724. doi: 10.1002/gj.3607.

Song MC, Li J, Yu XF, Song YX, Ding ZJ, Li SY. 2021a. Metallogenic characteristics and tectonic setting of the Jiaodong gold deposit, China. Solid Earth Sciences, 6(4), 385–405. doi: 10.1016/j.sesci.2021.07.002.

Song MC, Ding ZJ, Zhang JJ, Song YX, Bo JW, Wang YQ, Liu HB, Li SY, Li J, Li RX, Wang B, Liu XD, Zhang LL, Dong LL, Li J, He CY. 2021b. Geology and mineralization of the Sanshandao supergiant gold deposit (1200 t) in the Jiaodong Peninsula, China: A review. China Geology, 4(4), 1–34. doi: 10.31035/cg2021070.

Song MC, Ding ZJ, Liu XD, Li SY, L J, Dong LL, Wei XF, Bao ZY, Wang B, Zhang QB, Zhang LL, Liu HB, He CY. 2022a. Structural controls on the Jiaodong type gold deposits and metallogenic model. Acta Geologica Sinica, 96(5), 1774–1802 (in Chinese with English abstract). doi: 10.19762/j.cnki.dizhixuebao.2022143.

Song MC, Yang LQ, Fan HR, Yu XF, Ding ZJ, Zhang YW, Qiu KF, Li J, Zhang L, Wang B, Li SY. 2022b. Current progress of metallogenic research and deep prospecting of gold deposits in the Jiaodong Peninsula during 10 years for Exploration Breakthrough Strategic Action. Geological Bulletin of China, 41(6), 903–935 (in Chinese with English abstract). doi: 10.12097/j.issn.1671-2552.2022.06.001.

Tan J, Wei JH, Audétat A, Pettke T. 2012. Source of metals in the Guocheng gold deposit, Jiaodong Peninsula, North China Craton: Link to early Cretaceous mafic magmatism originating from Paleoproterozoic metasomatized lithospheric mantle. Ore Geology Review, 48, 70–87. doi: 10.1016/j.oregeorev.2012.02.008.

Tan J, Wei JH, Li YJ, Fu LB, Li HM, Shi WJ, Tian N. 2015. Origin and geodynamic significance of fault-hosted massive sulfide gold deposits from the Guocheng-Liaoshang metallogenic belt, eastern Jiaodong Peninsula: Rb-Sr dating and H-O-S-Pb isotopic constraints. Ore Geology Reviews, 65, 687–700. doi: 10.1016/j.oregeorev.2014.06.007.

Wallis S, Enami M, Banno S. 1999. The Sulu UHP Terrane: A review of the petrology and structural geology. International Geology Review, 41(10), 906–920. doi: 10.1080/00206819909465178.

Wang B, Song MC, Huo G, Zhou ML, Xu ZH, Jiang L, Song YX, Li J. 2021. Source characteristics and tectonic evolution of Late Mesozoic granites in Jiaodong and their implications for gold mineralization. Acta Petrologica et Mineralogica, 40(2), 288–320 (in Chinese with English abstract). doi: 10.3969/j.issn.1000-6524.2021.02.009.

Wang QF, Deng J, Wan L, Yang LQ, Gong QJ. 2007. Discussion on the kinetic controlling parameter of the stability of prebody distribution in altered rocks in the Dayingezhuang gold deposit, Shandong. Acta Petrologica Sinica, 23(4), 861–864 (in Chinese with English abstract). doi: 10.3969/j.issn.1000-0569.2007.04.018.

Wang ZC, Cheng H, Zong KQ, Geng XL, Liu YS, Yang JH, Wu FY, Becker H, Foley S, Wangyang C. 2020. Metasomatized lithospheric mantle for Mesozoic giant gold deposits in the North China craton. Geology, 48(2), 169–173. doi: 10.1130/G46662.1.

Wang ZL, Yang LQ, Deng J, Santosh M, Zhang HF, Liu Y, Li RH, Huang T, Zheng XL, Zhao H. 2014. Gold-hosting high Ba-Sr granitoids in the Xincheng gold deposit, Jiaodong Peninsula, East China: Petrogenesis and tectonic setting. Journal of Asian Earth Sciences, 95(1), 274–299. doi: 10.1016/j.jseaes.2014.03.001.

Wei YJ, Qiu KF, Guo LN, Liu XD, Tang L, Shi QF, Gao XK. 2020. Characteristics and evolution of ore fluids of the Dayingezhuang gold deposit, Jiaodong gold province. Acta Petrologica Sinica, 36(6), 1821–1832 (in Chinese with English abstract). doi: 10.18654/1000-0569/2020.06.11.

Wei YJ, Yang LQ, Feng JQ, Wang H, Lü GY, Li WC, Liu SG. 2019. Ore-fluid evolution of the Sizhuang orogenic gold deposit, Jiaodong Peninsula, China. Minerals, 9(3), 190–209. doi: 10.3390/min9030190.

Wei YJ, Yang LQ, Qiu KF, Wang SR, Ren F, Dai ZH, Li DP, Shan W, Li ZS, Wang JH, Tang L. 2022. Geology, mineralogy and pyrite trace elements constraints on gold mineralization mechanism at the giant Dayingezhuang gold deposit, Jiaodong Peninsula, China. Ore Geology Reviews, 148, 104992. doi: 10.1016/j.oregeorev.2022.104992.

Wen BJ, Fan HR, Hu FF, Liu X, Yang KF, Sun ZF, Sun ZF. 2016. Fluid evolution and ore genesis of the giant Sanshandao gold deposit, Jiaodong gold Province, China: Constrains from geology, fluid inclusions and H-O-S-He-Ar isotopic compositions. Journal of Geochemical Exploration, 171, 96–112. doi: 10.1016/j.gexplo.2016.01.007.

Wu L, Monié P, Wang F, Lin W, Ji WB, Yang LK. 2018. Multi-phase cooling of Early Cretaceous granites on the Jiaodong Peninsula, East China: Evidence from $^{40}Ar/^{39}Ar$ and (U-Th)/He thermochronology. Journal of Asian Earth Sciences, 160, 334–347. doi: 10.1016/j.jseaes.2017.11.014.

Xie TC, Dai CG, Li RX, Liu XD, Sui XL, Xue HH. 2022. New understandings of 3D feature and mineralization enrichment regularity in the Dayingezhuang-Caojiawa gold deposit of Jiaodong Peninsula. Geological Bulletin of China, 41(6), 986–992 (in Chinese with English abstract). doi: 10.12097/j.issn.1671-2552.2022.06.007.

Xu B. 1999. Geologic and Geochemical Characteristics of Dayingezhuang Gold Deposit in Shandong Peninsula, China. Tokyo, Technical School of Tokyo University, Ph.D thesis, 1 –139 (in Japanese with English abstract).

Yao XF, Cheng ZZ, Du ZZ, Pang ZS, Yang YQ, Liu K. 2021. Petrology, geochemistry, and Sr-Nd-S isotopic compositions of ore-hosting biotite monzodiorite in the Luanjiahe gold deposit, Jiaodong peninsula, China. Journal of Earth Science, 32(1), 51–67. https://doi.org/10.1007/s12583-020-1386-7.

Yue XF, Li DP, Tian JX, Yang DP, Shan W, Geng K, Xiong YX, Chi NJ, Wei PF, Liu PR. 2020. Deep gold mineralization features of Jiaojia metallogenic belt, Jiaodong gold Province: Based on the breakthrough of 3000 m exploration drilling. China Geology, 3, 385–401. doi: 10.31035/cg2020048.

Yang LQ, Deng J, Guo CY, Zhang J, Jiang SQ, Gao BF, Gong QJ, Wang

QF. 2009. Ore-forming fluid characteristics of the Dayingezhuang gold deposit, Jiaodong Gold Province, China. Resource Geology, 59(2), 181–193. doi: 10.1111/j.1751-3928.2009.00089.x.

Yang LQ, Deng J, Goldfarb RJ, Zhang J, Gao BF, Wang ZL. 2014a. $^{40}Ar/^{39}Ar$ geochronological constraints on the formation of the Dayingezhuang gold deposit: New implications for timing and duration of hydrothermal activity in the Jiaodong gold province, China. Gondwana Research, 25(4), 1469–1483. doi: 10.1016/j.gr.2013.07.001.

Yang LQ, Deng J, Wang ZL, Zhang L, Guo LN, Song MC, Zheng XL. 2014b. Mesozoic gold metallogenic system of the Jiaodong gold province, eastern China. Acta Petrological Sinica, 30(9), 2447–2467 (in Chinese with English abstract).

Yang LQ, Deng J, Guo LN, Wang ZL, Li XZ, Li JL. 2016. Origin and evolution of ore fluid, and gold-deposition processes at the giant Taishang gold deposit, Jiaodong Peninsula, eastern China. Ore Geology Reviews, 72, 585–602. doi: 10.1016/j.oregeorev.2015.08.021.

Yang LQ, Guo LN, Wang ZL, Zhao RX, Song MC, Zheng XL. 2017. Timing and mechanism of gold mineralization at the Wang'ershan gold deposit, Jiaodong Peninsula, eastern China. Ore Geology Reviews, 88, 491–510. doi: 10.1016/j.oregeorev.2016.06.027.

Yang LQ, Dilek Y, Wang ZL, Weinberg RF, Liu Y. 2018. Late Jurassic, high Ba-Sr Linglong granites in the Jiaodong Peninsula, East China: Lower crustal melting products in the eastern North China Craton. Geological Magazine, 155(5), 1040–1062. doi: 10.1017/S0016756816001230.

Yang SW. 1986. A discussion on the Jiaodong group strata, the source-bed of gold and the stratabound features of gold ore deposits in northwest part of Jiaodong Peninsula. Contributions to Geology and Mineral Resources Research, 1(2), 1–12 (in Chinese with English abstract). doi: 10.6053/j.issn.1001-1412.1986.3. 004.

Yu XF, LI DP, Tian JX, Shan W, Li HK, Yang DP, Zhang SK, Luo WQ, Xiong YX. 2018. Progress of deep exploration and theoretical innovation of metallogenic of gold deposits in Shandong Province. Shandong Land and Resources, 34(5), 1–13 (in Chinese with English abstract).

Yuan ZZ, Li ZK, Zhao XF, Sun HS, Qiu HN, Li JW. 2019. New constraints on the genesis of the giant Dayingezhuang gold (silver) deposit in the Jiaodong district, North China Craton. Ore Geology Reviews, 112, 103038. doi: 10.1016/j.oregeorev.2019.103038.

Zhai MG, Fan HR, Yang JH, Miao LC. 2004. Large-scale cluster of gold deposits in east Shandong: Anorogenic metallogenesis. Earth Science Frontiers, 11(1), 85–98 (in Chinese with English abstract). doi: 10.3321/j.issn:1005-2321.2004.01.005.

Zhang BL, Shan W, Li DP, Xiao BJ, Wang ZL, Zhang RZ. 2017. Hydrothermal alteration in the Dayingezhuang gold deposit, Jiaodong, China. Acta Petrologica Sinica, 33(7), 2256–2272 (in Chinese with English abstract).

Zhang J, Zhao ZF, Zheng YF, Dai MN. 2010. Postcollisional magmatism: Geochemical constraints on the petrogenesis of Mesozoic granitoids in the Sulu orogen, China. Lithos, 119(3–4), 512–536. doi: 10.1016/j.lithos.2010.08.005

Zhang L, Liu Y, Li RH, Huang T, Zhang RZ, Chen BH, Li JK. 2014. Lead isotope geochemistry of Dayingezhuang gold deposit, Jiaodong Peninsula, China. Acta Petrologica Sinica, 30(9), 2468–2480 (in Chinese with English abstract).

Zhang L, Weinberg RF, Yang LQ, Groves DI, Sai SX, Matchan E, Phillips D, Kohn BP, Miggins DP, Liu Y, Deng J. 2020. Mesozoic orogenic gold mineralization in the Jiaodong Peninsula, China: A focused event at 120±2 Ma during cooling of pregold granite intrusions. Economic Geology, 115(2), 415–441. doi: 10.5382/econgeo.4716.

Zhang LG, Chen ZS, Liu JX, Yu GX. 1994. Water-rock exchange in the Jiaojia type gold deposit: A study of hydrogen and oxygen isotopic composition of ore-forming fluids. Mineral Deposits, 13(3), 193–200 (in Chinese with English abstract).

Zhang LG, Chen ZS, Liu JX, Yu GX, Wang KF, Wang BC, Xu JF, Zheng WS, Li DY, Li H, Hou DY. 1995. Two-stage Water-rock Isotope Exchange Theory and Its Exploration Application. Beijing, Geological Publishing House, 1–220 (in Chinese).

Zhang QB, Song MC, Ding ZJ, Guo ML, Zhou ML, Dai CG, Huo G, Zhang P. 2022. Exhumation history and preservation of the Jiaojia giant gold deposit, Jiaodong Peninsula. Science China Earth Sciences, 65(6), 1161–1177. doi: 10.1007/s11430-021-9887-1.

Zhang RZ, Wang ZL, Wang SR, Liu Y, Qin WK. 2016. Metallogenic mechanism of Dayingezhuang gold deposit, northwestern Jiaodong Peninsula: Geochemistry constrains from the gold bearing pyrite typomorph and sulfur isotope. Acta Petrologica Sinica, 32(8), 2451–2464 (in Chinese with English abstract).

Zhang YQ, Dong SW, Zhao Y, Zhang T. 2008. Jurassic tectonics of North China: A synthetic view. Acta Geologica Sinica, 81(11), 1462–1480 (in Chinese with English abstract). doi: 10.3321/j.issn:0001-5717.2007.11.002.

Zhang YW, Hu FF, Fan HR, Liu X, Feng K, Cai YC. 2020. Fluid evolution and gold precipitation in the Muping gold deposit(Jiaodong, China): Insights from in-situ trace elements and sulfur isotope of sulfides. Journal of Geochemical Exploration, 218, 106617. doi: 10.1016/j.gexplo.2020.106617.

Zheng YF, Chen JF. 2000. Stable Isotope Geochemistry. Beijing, Science Press, 143–186 (in Chinese).

Zhu RX, Chen L, Wu FY, Liu JL. 2011. Timing, scale and mechanism of the destruction of the North China Craton. Science China Earth Science, 54, 789–797. doi: 10.1007/s11430-011-4203-4.